

Manuscript Number: SAA-D-18-01908R1

Title: Characterization of Eocene fossil resin from Moravia, Czech Republic: Insights into macromolecular structure

Article Type: Full Length Article

Section/Category: Analytical Spectroscopy and New Methods

Keywords: Amber; Fossil resin; Studlovite; ATR-FTIR; Py-GC/MS

Corresponding Author: Mrs. Martina Havelcová, Ph.D.

Corresponding Author's Institution: Institute of Rock Structure and Mechanics

First Author: Martina Havelcová, Ph.D.

Order of Authors: Martina Havelcová, Ph.D.; Vladimír Machovič; Alexandra Špaldoňová; Laidslav Lapčák; Jiří Hendrych; Martin Adam

Abstract: Two pieces of studlovite - Eocene amber from Študlov (South-east Moravia, Czech Republic) were investigated. To arrive at a more detailed description, attenuated total reflection Fourier transform infrared spectroscopy, Raman spectroscopy, pyrolysis-gas chromatography/mass spectrometry, and gas chromatography-mass spectrometry were used. Both studlovite samples revealed signs of the same plant source, with higher polymerisation and a higher degree of maturation of the fossilized matter. Despite their close spectral resemblance, they differed in their detailed chemical composition, and in structure. Layering of one of the pieces studied showed how the resin was built and what impact the process had on the chemical composition of the amber. Characterization of the organic matter was completed with an analysis of trace elements in amber samples using scanning electron microscope combined with elemental distribution analysis (SEM/EDAX). The results demonstrated the paleoenvironmental conditions that occurred in the plant during resin exudation following wounding.

Spectrochimica Acta A

Prague, January 21, 2019

Dear Editors

Please find attached the revised version of the manuscript SAA-D-18-01908 **“Characterization of Eocene fossil resin from Moravia, Czech Republic: Insights into macromolecular structure”** as well as the responses to reviewers comments (all suggestions have been implemented).

I would like to thank you for your consideration of the revised paper for publication, and thanks the reviewers for their thoughtful review, and for their valuable suggestions.

With best regards

Martina Havelcová
(corresponding author)

Contact address:

Institute of Rock Structure and Mechanics
The Czech Academy of Sciences
CZ-182 09 Prague 8
Czech Republic
e-mail: havelcova@irms.cas.cz

Reviewer #1:

1. The abstract uses the term "Fourier Transform" twice, line 3 and 4. This should be "Fourier transform"

The terms in the abstracts were corrected.

2. Paragraph 3, line one, should be "...scanning from m/z 20 to 500...."

The error was corrected.

3. Figure 9A/B "biphenyles" should be "biphenyls"

The error was corrected.

4. Differences between the between the levels of elements reported from EDX are small, with the levels of the elements in Table 3 and variation in figure 8A and 8B being max 1-2 %. How significant are these variations, i.e. what is the error of measurement and how was it determined? This is important to make deductions on variations over layers and should be reported on.

To support precisions of EDX analyses, the software was calibrated for quantification using pre-measured universal standards included in the EDX software, and data sets consisted of 10 replicate measurements. The RSD was supplemented for every value in the table 3.

There are no doubts that there are alternative techniques which are more precise, but the advantages of SEM-EDX technique (the small sample size needed and no pretreatment) prevailed.

5. It is not clarified if the percentages reported or mol % or weight %. This is important for the significance of detection as well.

Percentages were completed for clarification.

6. The use of IR band ratios is reported on extensively, however the rationale is not explained or explicitly referenced to a previous paper in the section '3. Results' as to why the 1446 cm⁻¹ band normalization is done. A fleeting comparison is made to previously reported ratios to the end of paragraph one, of section '4. Discussion', however a better explanation/reference in the preceding results text should be made.

The most characteristic bands in the spectra is feature about 1446 cm⁻¹, which may be assigned to the intensity of aliphatic C-H bonds deformation. The band is useful and commonly used as „inert standard“ because remains almost constant. A reference was added into the text of the section 3. Results.

7. Assignments of IR bands are made in the text and extensively in Table 2. The experimental section reports that IR data were collected from 650-4000 cm⁻¹, however Table 2 makes assignments from 310 cm⁻¹. How was this done?

The range 650-4000 cm⁻¹ is connected with ATR-FTIR method (left columns in the Table 2). The assignments from 310 cm⁻¹ is for FT-Raman method. The experimental section was completed by range of Raman data were collected: 3500-50 cm⁻¹.

8. The assignments in Table 2 are very detailed, are these assignments accurate or rather refer to potential origin, as it contains assignments to S-S bonds (519, 555 and 556 cm⁻¹), with no sulphur containing molecules were detected in any of the analyses. Table 2 should be reviewed for accuracy and referenced accordingly.

The bands in the infrared and Raman spectra were specified according to Guiliano et al., 2004; Jehlička et al., 2004; Brody et al., 2001; Socrates, 1994; Beck et al., 1964. These references were added to the table caption.

9. A legend explaining what <upsilon>, <delta> and <rho> are in Table 2 should be added.

The legend for Table 2 was completed: ν - stretching, δ - deformation vibration, γ - out-of-plane, ρ - rocking, a - asymmetric, s - symmetric, ar - aromatic ring

Reviewer #2: Characterization of Eocene fossil resin from Moravia, Czech Republic:
Insights into macromolecular structure

- The introduction was written in a short manner depending on 8 references.

Due to the limited knowledge and publications on the studied fossil resin, the number of references is low.

- Materials and methods were described well -Results

* I see that FT-Raman spectra of studlovite I (A) and studlovite II (B) (Fig. 5) must be inserted before the Curve fitted ATR spectra of studlovite I (A) and studlovite II (C), and curve fitted Raman spectra of studlovite I (B) and studlovite II (D) (Fig. 4).

That is right, and the spectra were moved.

* the last percentage in table (3) is for P (phosphorus which was no mentioned in the result or discussion) or Pb (lead) and if it is for Pb this percentage value (1.18) is average of 8 layers of studlovite II (as the authors mentioned), while the minimum percentage value of Pb for studlovite II as show in (Fig, 8B) is about 2.75 and its average percent for 8 layers dose not equal to that reported value in the table 3.

Unfortunately, the table was not fully visible in the load manuscript. I hope that now it is OK.

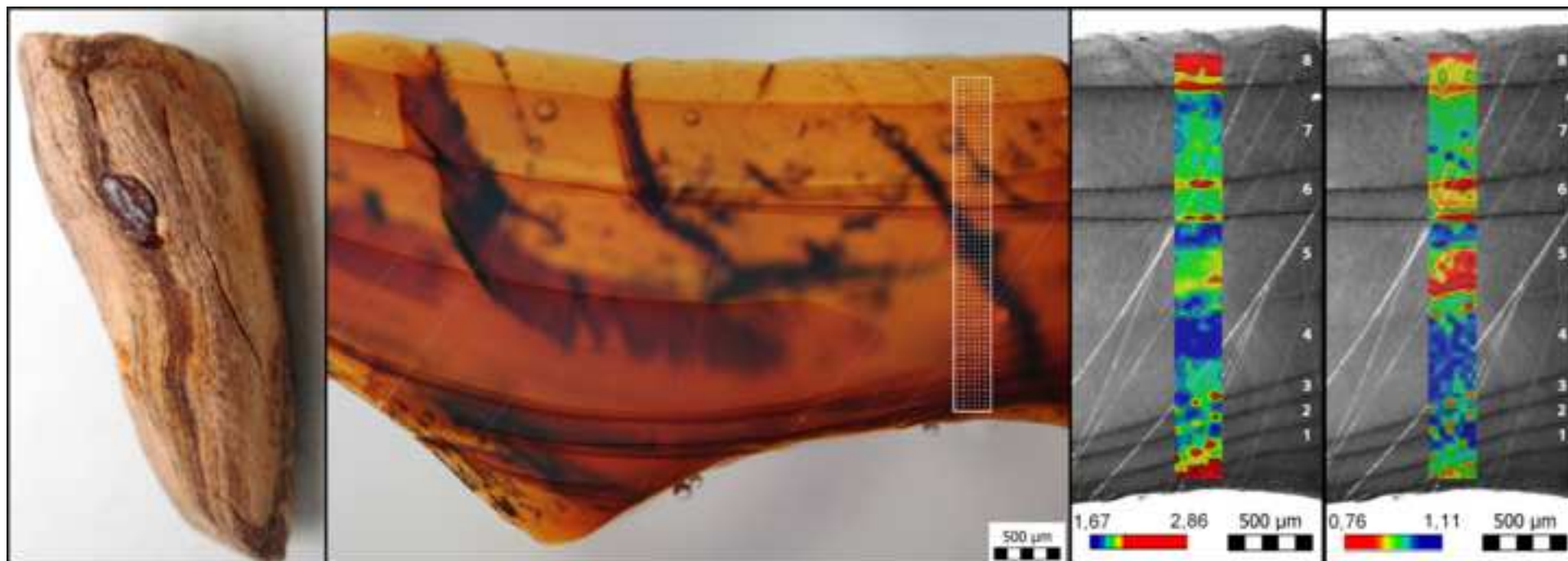
*Diisopropylmethylbenzene, diisopropylxylene Tetrahydrotrimethylnaphthalene, diacetyldiphenylmethane and tetramethylphenanthrene are recorded in table (1) while there are no lables for them in Fig (2).

The lables for the mentioned compounds were added to the figure.

*Fig 7

The labels titles of histogram are COOH and COOR what is R represent ?

R could represent aliphatic substituent or polymolecular fragment, and this explanation was added to the figure caption.



*Highlights (for review)

- Two pieces of studlovite amber were analysed
- Spectroscopic fingerprints were obtained along with the composition of extracts
- Layers within the amber were documented and chemically characterized
- Trace elements in bulk samples and in the layers were determined

Characterization of Eocene fossil resin from Moravia, Czech Republic: Insights into macromolecular structure

Martina Havelcová^{a,*}, Vladimír Machovič^{a,b}, Alexandra Špaldonová^a, Ladislav Lapčák^b,
Jiří Hendrych^b, Martin Adam^c

^a *Institute of Rock Structure and Mechanics AS CR, V Holešovičkách 41, 182 09 Prague 8, Czech Republic*

^b *Institute of Chemical Technology Prague, Technická 5, 166 28 Prague 6, Czech Republic*

^c *University of Pardubice, Faculty of Chemical Technology, Studentská 573, 532 10 Pardubice, Czech Republic*

1. Introduction

The Eocene epoch is known as a source of abundant accumulations of Baltic amber. This amber was transported from coastal areas of Northern Europe to the Mediterranean Sea in ancient times. The trade road, called the Amber Road, crossed the territory of Moravia, which has supported rich archaeological finds of amber [1,2]. However, next to Baltic amber, other amber occurrences were documented from deposits lying in Moravia, an area integral to the Czech Republic [3].

One of the Eocene amber deposits in Moravia is from the Carpathian Flysch Belt. This amber was entitled studlovite, according to its site of discovery at the village of Študlov, near Valašské Klobouky. Historically, findings of pieces of relatively high weight (> 40 grams) and up to 8 cm in size have been documented in the locality. Nowadays, occurrences are scarce. Colour and quality resembles Baltic amber, and the rare occurrence of suffused insects has also been documented [4].

Studlovite has been analysed in the past and it has been suggested that an angiosperm plant was the source of this amber [5]; a relationship with Baltic amber has also been proposed [6]. The most recent description of studlovite material [7,8] has revealed a chemical composition rather similar to that of the Cenomanian amber from Nové Strašecí.

Generally, amber is derived from exudates of conifers and certain angiosperms, and represents a valuable source of information about its botanical origins, ancient terrigenous ecosystems or distribution conditions. However, biochemical fingerprints of original resins have been modified during diagenesis, therefore the chemical analysis of amber is not straightforward. Biomarkers of fossil resins are terpenoids, and among them, specific terpenoids representing one plant family have the highest chemotaxonomic value. Such an identifying terpenoid has not been found for Študlov amber and doubts about the source of the original plant material still persist.

A more comprehensive geochemical analysis of the amber is therefore needed in order to evaluate the original plant source and the fossilization process. The aim of this study was to determine the molecular composition of Študlov amber using attenuated total reflection Fourier transformed infrared spectroscopy (ATR-FTIR), and Fourier transformed Raman spectroscopy, together with gas chromatography/mass spectroscopy and pyrolysis–gas chromatography/mass spectrometry (GC/MS and Py-GC/MS). Environmental scanning electron microscopy coupled with energy-dispersive X-ray analysis (SEM/EDAX) provided information on the elements present in the organic matter.

2. Materials and methods

2.1. Samples

The studlovite samples (studlovite I, studlovite II) were found in deep-sea sediments in a site formed by russet clay sandstone (Fig. 1). Amber pieces examined in this study were small in size ($0.5 \times 0.5 \times 0.5$ cm). The samples were brown in colour, partly transparent, one of them (studlovite II) having visible layers. They exhibited similar elemental compositions, having 69.7 wt% C, 8.1wt% H, and below 0.1 wt% of N and S.

The locality of fossil resin at Študlov in eastern Moravia is a part of the Outer West Carpathians, which are made of Mesozoic and Tertiary flysch formations, the Carpathian Flysch Belt, and the locality lies in the deep-sea sediments of the Beloveža formation of the Račanská unit. The geological composition of the Račanská unit includes stratified sandstone, alternating with a conglomerate and inter-layered clay-slate, green-grey and red-brown claystone (upper Eocene, lower Oligocene).

2.2. Methods

The elemental organic composition of crushed and homogenized samples was determined using a CHNS/O micro-analyzer (Thermo Finnigan Flash FA 1112).

The sample (cca 0.2 mg) was dissolved in dichloromethane and analyses were performed using a Trace GC Ultra-DSQ II (ThermoElectron) instrument equipped with a TR-5MS column ($60\text{m} \times 0.25\text{mm} \times 0.25\mu\text{m}$). The oven temperature was programmed from 40 °C (1 min) to 120 °C (15 °C/min), to 200 °C (10 °C/min), then to 300 °C (10 min) (20 °C/min). The sample extracts were injected in splitless mode, the injector temperature was set at 220 °C and helium was the carrier gas. Mass spectra were obtained by scanning from m/z 20 to 500 in full scan mode. For data processing, the Xcalibur software (ThermoElectron) was used. Components were assigned from retention times and comparisons with mass spectra from the National Institute of Standards and Technology spectral library. Selected ion monitoring (SIM) was also used as a mode of data acquisition. The area of each individual peak was divided by the total area of the integrated TIC and expressed as the relative abundance of the total area in percent.

Py-GC/MS analyses were performed using a Pyroprobe 5150 pyrolysis unit (CDS Analytical) connected to the GC/MS instrument described above. Samples of fossil resins were heated at 400 °C for 20 s. This temperature was chosen based on experimental results (see Supplemental material S1). The Py-GC interface was kept at the maximum allowed temperature of 350 °C. A TR-5MS column was used and the temperature program of the column was set from 40 to 120 °C at a rate of 20 °C/min, continued at a rate of 8 °C/min to 210 °C, and finished at a rate of 20 °C/min to 300 °C, holding for 5 minutes.

Micro-ATR-FTIR analysis (ATR mapping) employed a Nicolet 6700 spectrometer (Thermo Nicolet Instruments Co.) combined with a Thermo Continuum IR microscope. The system was equipped with a X-Y-Z motorised stage with incremental steps of 1 μm . A polished section was placed on the microscope stage and the area of investigation ($280 \times 3400 \mu\text{m}$) was selected through a 15 x objective. Spectra were acquired over a wavenumber range of $4000\text{-}650 \text{ cm}^{-1}$, from 64 scans, at a spectral resolution of 4 cm^{-1} . An ATR germanium crystal directly connected to the objective was used, resulting in investigated areas of about $40 \times 40 \mu\text{m}$. A step size of $40 \mu\text{m}$ was used (588 points were measured). Data collection and post-run processing were carried out using Nicolet Omnic AtIus imaging software.

FT-Raman spectra were obtained using a Nicolet 6700 instrument with the NXR 9650 FT-Raman module attached and $\text{Nd}^{3+}/\text{YVO}_4$ near infrared excitation at 1064 nm. Spectra were acquired over a

wavenumber range of 3500-50 cm^{-1} , and recorded at 4 cm^{-1} resolution from 1024 accumulated scans. A nominal laser power of about 0.1W was used with a spot size of 50 μm .

A Quanta 450 scanning electron microscope (SEM) was used to study the samples. The semi-quantitative chemical compositions of the samples were analysed using an energy-dispersive X-ray microanalyser (EDAX, Apollo X) attached to the SEM, with a 12.5kV excitation electron beam. The analysis was carried out on selected spots of the cut surface prepared from the samples.

3. Results

3.1. Qualitative characteristic of bulk samples

The Py-GC/MS method utilized heat to release all volatiles and to degrade compounds from their solid state by thermal cracking or hydrogen abstraction reactions. The results of Py-GC/MS analysis (Fig. 2) were close for both samples: a set of cyclo-compounds and *n*-alkanes were the products of thermal reactions, and other substituted benzene, naphthalene, and phenanthrene compounds were products of bond breaking fragmentation reactions. The fragments produced are assumed to be representative of the original non-volatile compounds. Megastigmatrienone and ionone were identified only in pyrograms of studlovite II.

The infrared microspectra of the two study samples (Fig. 3) showed marked differences in band intensities of oxygen functional groups in the spectral range between 3700 and 3100 cm^{-1} , where a broad envelope of hydroxyl groups stretching vibrations of alcohols and phenols was found. Band positions at 3460 and 3225 cm^{-1} indicated the presence of hydroxyl groups with different hydrogen bonding strengths. A higher content of these OH groups was detected in studlovite I.

The representative Raman spectra of the two amber samples analyzed were qualitatively similar (Fig. 4), and differed mainly in the intensities C-H and C=C bonds. The spectral range of 1830-1500 cm^{-1} , as for the infrared spectra, was curve fitted using the Gaussian-Lorentzian function (Fig. 5 B, D, and Table 2). Bands of carbonyl functional groups (~ 1670 , ~ 1700 and 1725 cm^{-1}), double bonds (1650 cm^{-1}) and aromatic C = C bonds (~ 1610 and $\sim 1570 \text{ cm}^{-1}$) were detected in this region.

Bands of stretching vibrations of carbonyl groups and C = C bonds were determined in the spectral region 1800-1500 cm^{-1} . For a more detailed analysis, this region was curve fitted using a mixed Gaussian-Lorentzian function (Fig. 5 A,C). Both samples contained two distinct bands of ketones/H-bonded esters at 1724 cm^{-1} , and carboxylic acids at $\sim 1700 \text{ cm}^{-1}$. The relative proportions of these functional groups were determined based on intensities related to the intensity of the deformation vibrations of the aliphatic C-H bonds at 1446 cm^{-1} (i.e., I_{1724}/I_{1446} and I_{1700}/I_{1446}) [9]. Ketones/ H-bonded esters had almost the same representation in both samples, whereas the COOH group content was almost doubled in the studlovite I. These data were obtained by scanning of polished sections over entire sample profiles, and secondary surface oxidation of the samples can be excluded. The bands of anhydrides (1770 cm^{-1}), conjugated carbonyls (1664 cm^{-1}), double C = C bonds (1642 cm^{-1}) and C = C aromatic rings ($\sim 1600 \text{ cm}^{-1}$) were also identified (Table 2).

Stretching vibrations of aliphatic C-H bonds in CH_3 , CH_2 , and CH groups were found in the range 3000-2700 cm^{-1} . The corresponding area of deformation vibrations was located at ~ 1450 and $\sim 1380 \text{ cm}^{-1}$. A relatively large number of overlapping bands in the 1300-900 cm^{-1} region belonged predominantly to stretching vibrations of C-O bonds in acids, phenols, alcohols and esters. Next to these were bands of deformation vibrations of OH and CH bonds, and stretching vibrations of ring C-C bonds.

Despite the organic origin of amber, the material also contained inorganic elements, as was demonstrated by SEM/EDAX analysis (Table 3).

There were differences between the samples in higher levels of Fe, Al, and Si in studlovite I, and higher levels of Pb in studlovite II.

3.2. Layer-by-layer amber characterisation

Microphotographs of studlovite II enhanced layers present in the amber structure are shown (Fig. 6A). A suitable rectangular area was sketched, with dimensions of 280 x 3400 μm and with 504 points. The area contained eight layers of irregular thickness ranging from 120 to 560 μm that were 2D mapped by infrared ATR microspectroscopy.

The spectra obtained on the layer boundaries demonstrated the presence of significantly higher concentrations of oxygen containing functional groups than regions within layers. Moreover, the specific band for carboxylic acids indicated their higher presence on the boundaries. Semi-quantitative aspects of the FTIR analysis was presented as ratios of the integrated areas of carbonyl groups, including aldehydes, ketones, carboxylic acid, carboxylate esters and anhydrides (1800-1540 cm^{-1}), and aliphatic bonds, represented by δ -CH deformation modes (1505-1405 cm^{-1}). For the detailed distribution of oxygen containing functional groups, the carbonyl groups in ketones/H-bonded esters (1720 cm^{-1}) and in carboxylic acids (1695 cm^{-1}) were applied as well. The resulting representations of the area ratio $A_{\text{C=O}}/A_{\text{C-H}}$ (Fig. 6B) and intensity ratio I_{1720}/I_{1695} (Fig. 6C) followed and highlighted the layer boundaries, showing that oxygen containing groups, specifically carboxylic acids, were present in higher concentrations on the layer interface. The material in regions between layers of the fossil resins was richer in aliphatic chains and ketonic C=O bonds.

From the profile, the highest concentrations of carbonyl groups were observed on both outside layers of the pieces studied, and therefore eight average spectra from the eight individual layers and the $I_{\text{C=O}}/I_{\text{C-H}}$ ratios were used for a more detailed analysis. The layer profile showed that the ketone/H-bonded ester concentrations were relatively constant in all layers while the concentration of carboxyl groups changed, with the highest concentrations occurring in the outer layers, and the lowest in the middle 4 to 6 layers (Fig. 7).

Layers of a piece of studlovite II also showed differing inorganic chemical signatures (Fig. 8A). The distribution of Na, Mg, Al, Si, and Fe was comparable among the layers with an important decrease in the fifth layer. But the inorganic signals in layers were different for Cu and Pb, which seemed to be quite homogeneous through the sample (Fig. 8B).

3.3. Solvent extract analysis

Samples had low extractability in dichloromethane: 3.6wt%, and 5.1wt% respectively.

The studlovite II sample extract contained high concentrations of aromatic compounds (65%), comprising substituted naphthalenes, biphenyls and phenanthrenes (Fig. 9 B, Table 4). C_1 - C_4 methyl naphthalenes were dominant (46%) together with methylbiphenyls (15%). The saturated hydrocarbons included mainly *n*-alkanes (25%) with their distribution in the range from *n*- C_{10} to *n*- C_{28} , and with lower *n*-alkanes dominating with a maximum at *n*- C_{11} . The acyclic isoprenoid pristane (Pr) was also identified. The composition of the studlovite I sample extract differed noticeably from studlovite II with a very weak contribution of all compounds (Fig. 9 A, Table 4).

Selected ion monitoring enabled the detection of minor concentrations of compounds with a terpenoid skeleton from the original resin source. The composition of both extracts included ionene, methylionenes, cadalene, 8 β (H)-labdane, and simonellite. The extract of studlovite I also contained an unknown sesquiterpene with a molecular weight of 204, and the studlovite II extract contained 1,4-dimethyladamnatane (C_{12} adamantane), 5,6,7,8-tetrahydrocadalene (calamene), and retene.

4. Discussion

Amber is a fossilized tree resin and its chemical structure can be quite complex and diverse, and being of a resinous nature, is more or less soluble in an organic solvent. As amber matures over years, additional polymerization and isomerization reactions take place, as well as crosslinking and cyclization. The FTIR and Raman spectral data from analysis of the macromolecular structure of bulk studlovite II revealed the presence of carboxyl, hydroxyl, and ketone or H-bonded ester functional groups as well as single and double bonds. Generally, some spectral bands characterize the degree of maturation or degradation of an amber sample based on determinations of oxygen functional groups and the relative abundance of aliphatic and aromatic structures [10]. An indicator of immaturity is the Raman band at about 1650 cm^{-1} , assigned to the C=C stretching vibration of double bonds in methylene groups, because the elimination and loss of these bonds are the result of cross-linking of the resin material or by oxidative and maturation processes. The other important Raman band, revealing aliphatic C-H bending, appears at about 1450 cm^{-1} . The intensity ratio of the 1650 and 1450 cm^{-1} bands was suggested to indicate the degree of maturation. Jehlička et al. [9] found that values of this ratio ranged between 0.48 and 0.81 for fossil resin specimens, differing in localities, paleoecological situations and geological ages, including Bohemian and Moravian fossil resins and Baltic (Eocene) and Lebanon (Cretaceous) ambers. The studlovite samples studied showed I_{1650}/I_{1450} ratio values that were noticeable lower, at 0.31, and 0.39 respectively, showing a higher degree of polymerisation and maturation of these samples.

Next to the loss of double bonds in methylene groups, the fossilization of natural resins is accompanied by an increase in aromatic structures. Considering I_{1610}/I_{1450} ratios representing the presence of aromatic C=C bonds, this ratio was more than 10 % higher for studlovite I, showing the differential and higher degree of oxidation/maturation in comparison with studlovite II. The content of carboxylic groups in bulk samples was also much higher (44%) in studlovite I than in studlovite II, as was visible in curve fitted ATR-FTIR spectra (Fig. 3A and C), showing a broader band at 1700 cm^{-1} that was caused mainly by intermolecular H bonds in OH and COOH groups.

Remarkably similar differences in composition and maturation were observable from GC/MS analyses of amber extracts, despite the fact that studlovite I was less soluble in dichloromethane and the extract was poorer in compounds, indicating a higher degree of polymerization. The prevailing compounds, identified in both extracts, were nonspecific for chemotaxonomy, but slight traces of terpenoid compounds were detected: the sesquiterpenoid cadalane belongs to a class that is a common constituent of conifers; $8\beta(\text{H})$ -labdane is a part of bicyclic diterpenoids produced mainly by conifers, although they can also occur in angiosperms [11]; ionene and methyl ionene may be derived from labdanes during degradation processes; the adamantane skeleton of 1,4-dimethyladamnatane is the basic unit of diamondoids (geosynthetic compounds), and seems to originate from β -ionone, *n*-alkanes and polycyclic hydrocarbons, as was proven by synthesis under laboratory conditions from these organic precursors [12,13]. Aromatic biomarkers simonellite and retene are derived from compounds with tricyclic/tetracyclic compounds with abietane or phyllocladane carbon skeletons that commonly occur in both angiosperms and gymnosperms. Low concentrations of terpenoid compounds and the presence of components that are highly degraded diagenetic products without chemotaxonomic value are not sufficient evidence to assess the botanical source of the studlovite samples.

The natural precursors of studlovite were suggested to be deciduous trees [5], however this assumption was made on the basis of a missing succinic acid peak in the FTIR spectra and the presence of oleanane in the extract. The absence of angiosperm triterpenoids in studlovite I and studlovite II extracts rather demonstrated conifers to be the source of the amber. Modern plant families reported in the literature as possible sources of amber for the Eocene age are Araucariaceae, Cupressaceae s.l., Pinaceae and Podocarpaceae [14]. Py-GC/MS was primarily used to differentiate

and classify fossil resins [15]. Cyclo-compounds, *n*-alkanes, substituted benzene, naphthalene, phenanthrene compounds, as well as megastigmatrienone and ionone are fragments from terpenoid structures that formed the macromolecular amber matrix [16,17] and were fragmented through cracking reactions during pyrolysis. These compounds are nonspecific and it is hardly possible to use these data to conclude the origin of a resin. It can only be suggested that studlovite belongs to amber classification Class 2 due to the presence of methyl-naphthalenes and traces of cadalene and 8 β (H)-labdane.

Warm and humid conditions could increase resin exudation, as is known from recent forests in a warm subtropical or tropical climate. Studlovite is of Eocene age when northern European land was characterized by stable subtropical-tropical climates and the warmest climate in the Cenozoic Era. Resin, produced inside plants, was exuded from the plant (in direct defense against herbivores and pathogens or by physical damage), and accumulated on the trunk or limbs. Then it either dropped to the soil or remained within the secretory tissue of the tree, preserved within the trunk that became fossilized in the protective soil environment [14]. The transformation of resin into amber continues from the moment of secretion until its burial. Layers of resin can build up and harden to form amber fossil and amber pieces that have layers of diverse thickness, representing individual resin flows. They often contain remnants of insects that were trapped in its sticky embrace. Nel and Prokop [18] and Tkoč et al. [4] described Scatopsidae and Dolichopodidae (Insecta: Diptera) in Študlov amber. Layers with an irregular thickness were microscopically identified in studlovite II (Fig. 3). The layers can be assumed to have accrued *in situ* and not during sedimentation processes without access to air because of variations found at interfaces especially the presence of oxygen-containing functional groups.

Two types of oxidative degradation that had occurred during resin fossilization can be recognised in studlovite II thanks to the detailed layer analysis of this amber. The first process was primary oxidation that was expressed as the enrichment of carboxylic groups found on boundaries between layers (Fig. 6C). It seems that the time between individual resin flows was sufficient for the hydrolysis of esters on the open resin surface, as was characterised by higher intensities of the specific band for carboxylic acids relative to carbonyl groups [19]. Moreover, the carbonyl stretching vibration at 1720 cm⁻¹ was at a lower frequency than typically seen in aliphatic esters and this may be due to the polymeric structure of the resinite. The complex macromolecular structure could, for example, allow hydrogen bonding between ester and adjacent alcohol groups, thus lowering the carbonyl stretching frequency [20]. The secondary oxidation process, revealed in averaged spectra from the individual layers as decreasing concentrations of carboxylic groups towards the centre layer of the fossil resin, can be attributed to diffusion of the oxidation medium (air, water) into the reaction system.

After resin secretion, a first contact was with rainwater and eventually with seawater droplets that sprinkled the resin stuck on the tree trunk or covered in the forest litter. Sodium is assumed to be a typical marine element but no enrichment was observed in the samples, indicating that the inorganic signature was not influenced by a saline environment during amber formation, although sedimentological evidences indicated that the investigated samples were deposited in a deep-sea environment. Most of the elements determined, such as macro and micro nutrients, elements sensitive to redox conditions or those related to siliciclastic sources (Na, Mg, K, Fe, Si, Al) can be interpreted in terms of natural plant parts and biological processes. Being located beneath the soil, they were absorbed by plants and the resin composition can then be influenced by soil composition. The distribution of inorganic elements in layers of studlovite II (Fig. 8A) showed that the concentrations of Na, Mg, Fe, Si, and Al reflected resin secretion that was gradually produced and affected by different conditions within the tree and in the soil. The interesting finding was the high lead content in studlovite II, without a significant fluctuation in concentration within the layers. In sedimentary rocks, lead distribution is controlled by the presence of primary detrital minerals (feldspar, mica, and sulphides), clay minerals and organic matter. Lead has a strong affinity for organic ligands and could

be adsorbed onto the reactive surface sites on resin surfaces. The sorption might be attributed to resin carbohydrates and phenolic compounds that have metal-binding functional groups such as carboxyl and hydroxyl groups [21].

5. Conclusion

Analysis of the results showed that both studlovite samples were derived from the same plant source, with higher polymerisation and maturation of the fossilized matter. The samples alone, however, displayed differences in structure and chemical composition (Table 5). These variations could be ascribed to dissimilar processes when the structure of studlovite II was built by continuous resin layering that affected the resulting chemical composition of the amber. However, the final fossilisation of both samples lead to material with many nonspecific paleotaxonomic characteristics. Trace elements in amber samples could only demonstrate the paleoenvironmental conditions that existed in plants during resin exudation following wounding.

Acknowledgements

The work was carried out thanks to the Operational Program Prague—Competitiveness, project Centre for Texture Analysis (CZ.2.16/3.1.00/21538), and to the long-term conceptual development of research organisation RVO: 67985891. The authors are grateful to John Brooker for reviewing and correcting the manuscript.

References

- [1] V. Mátl, To the provenience of amber in archaeological excavations in Moravia, *Minerál* 1/93, (1993) 21 (in Czech).
- [2] I. Mrázek, Gemstones in prehistoric times in Moravia and Silesia, *Moravian Museum in Brno* 203 (1996) (in Czech, English summary).
- [3] M. Přichystal, Bernsteinbearbeitung in der hallstattzeitlichen Siedlung der Lausitzer Urnenfelderkultur in Kralice na Hané (Bez. Prostějov), *Urnfield and Hallstatt Periods, Contributions to the IXth conference in Bučovice 3.- 6. 10. 2006*, pp. 209–230 (in Czech, German summary).
- [4] M. Tkoč, A. Nel, J. Prokop, Discovery of a new species of the Cretaceous genus *Microphorites* Hennig, 1971 (Diptera: Dolichopodidae s. lat.) in Paleogene amber from eastern Moravia (Czech Republic), *Insect Syst. Evol.* 47 (2016) 181–193.
- [5] V. Mátl, J. Franců, Z. Boháček, O. Krejčí, Occurrence of amber in Študlov locality (Bílé Karpaty Mts., Moravia), *Bulletin mineralogicko-petrologického oddělení Národního muzea v Praze*, VII (1999) 179–183 (in Czech).
- [6] M. Ručka, P. Sláma, Unknown gemstone - retinit from Valašské Klobouky, *Minerál* 2/97 (1997) 115–121 (in Czech).
- [7] M. Havelcová, I. Sýkorová, K. Mach, Z. Dvořák, Organic geochemistry of fossil resins from the Czech Republic, *Procedia Earth and Planetary Science* 10 (2014) 303–312.
- [8] M. Havelcová, V. Machovič, M. Linhartová, L. Lapčák, A. Přichystal, Vibrational spectroscopy with chromatographic methods in molecular analyses of Moravian amber samples (Czech Republic), *Microchem. J.* 128 (2016) 153–160.

- [9] J. Jehlička, S.E. Jorge Villar, G.H.M. Edwards, Fourier transform Raman spectra of Czech and Moravian fossil resins from freshwater sediments, *J. Raman Spectrosc.* 35 (2004) 761–767.
- [10] C.W. Beck, E. Wilbur, S. Meret, Infra-red spectra and the origin of amber, *Nature* 201 (1964) 256–257.
- [11] A. Otto, V. Wilde, Sesqui-, di- and triterpenoids as chemosystematic markers in extant conifers – a review, *Bot. Rev.* 67 (2001) 141–238.
- [12] L. Berwick, R. Alexander, K. Pierce, Formation and reactions of alkyl adamantanes in sediments: carbon surface reactions, *Org. Geochem.* 42 (2011) 752–761.
- [13] A. Ma, Advancement in application of diamondoids on organic geochemistry, *J. Nat. Gas Geosci.* 1 (2016) 1–9.
- [14] J.H. Langenheim, *Plant resins*, Timber Press, Inc., Potland, Oregon, 2003.
- [15] K.B. Anderson, R.E. Winans, Nature and fate of natural resins in the geosphere. I. Evaluation of pyrolysis-gas chromatography mass spectrometry for the analysis of natural resins and resinates. *Anal. Chem.* 63 (1991) 2901–2908.
- [16] G. Fráter, J.A. Bajgrowicz, P. Kraft, Fragrance chemistry, *Tetrahedron* 54 (1998) 7633–7703.
- [17] M.-F. Nonier, N.V. De Gaulejac, N. Vivas, C. Vitry, Characterization of carotenoids and their degradation products in oak wood. Incidence on the flavour of wood, *CR Chim.* 7 (2004) 689–698.
- [18] A. Nel, J. Prokop, New Paleogene Scatopsidae (Diptera: Nematocera) in amber from the Czech Republic and France. *Acta Societatis Zoologicae Bohemicae* 68 (2004) 91–98.
- [19] G. Pastorelli, Y. Shashoua, J. Richter, Hydrolysis of Baltic amber during thermal ageing – An spectroscopic approach. *Spectrochim. Acta A* 106 (2013) 124–128.
- [20] G. Socrates, *Infrared and Raman characteristic group frequencies: Tables and chart*, 3rd ed., Wiley & Sons, 2004.
- [21] A.E. Ofomaja, E.B. Naidoo, Biosorption of lead(II) onto pine cone powder: Studies on biosorption performance and process design to minimize biosorbent mass, *Carbohydr. Polym.* 82 (2010) 1031–1042.
- [22] M. Guiliano, L. Asia, G. Onoratini, G. Mille, Applications of diamond crystal ATR FTIR spectroscopy to the characterization of ambers, *Spectrochimica Acta A* 67 (2007) 1407–1411.
- [23] R.H. Brody, H.G.M. Edwards, A.M. Pollard, A study of amber and copal samples using FT-Raman spectroscopy, *Spectrochimica Acta A* 57 (2001) 1325–1338.

Figure captions

Fig. 1. A - Amber piece at the exposure of the clay sandstone; B - studlovite I; C - studlovite II: layers are obvious in this transparent amber.

Fig. 2. Total ion pyrograms of studlovite I and studlovite II. The list of all identified compounds is in Table 1. The numbers above peaks indicate carbon numbers of *n*-alkanes, DMB - dimethylbenzene, TMB - trimethylbenzenes, DEB - diethylbenzene, N - naphthalene, MN - methylnaphthalenes, B - biphenyl, DPMB - diisopropylmethylbenzene, DPX - diisopropylxylene, M - megastigmatrienone, I - ionone, TeHP - tetrahydrotrimethylnaphthalene, diAdiPM - diacetyldiphenylnaphthalene, TeMP - tetramethylphenanthrene.

Fig. 3. ATR-FTIR microspectra of studlovite I and studlovite II. The list of bands and their assignments is in Table 2.

Fig. 4. FT-Raman spectra of studlovite I (A) and studlovite II (B). The list of bands and their assignments is in Table 2.

Fig. 5. Curve fitted ATR spectra of studlovite I (A) and studlovite II (C), and curve fitted Raman spectra of studlovite I (B) and studlovite II (D). The list of bands and their assignments is in Table 2.

Fig. 6. A - Microphoto of a studlovite II amber piece with the area studied and 504 measured points (280 x 3400 μm), B - ATR-FTIR profile $A_{\text{C=O}}/A_{\text{C-H}}$ (1800-1540 cm^{-1} /1505-1405 cm^{-1}), C - ATR-FTIR profile I_{1720}/I_{1695} . (The white lines on B and C arose during sample cutting and polishing.)

Fig. 7. Relative representation of esters (1720 cm^{-1}) and carboxylic acids (1695 cm^{-1}) obtained using $A_{\text{C=O}}/A_{\text{C-H}}$ (1800-1540 cm^{-1} /1505-1405 cm^{-1}) ratios from averaged curve-fitted spectra in individual layers. R = aliphatic substituent or polymolecular fragment

Fig. 8. Distribution of inorganic elements within the layers of studlovite II.

Fig. 9. Total ion chromatograms (TIC) of studlovite I (A) and studlovite II (B) extracts, and selected ion monitoring chromatograms for *n*-alkanes (m/z 85), naphthalenes (m/z 128+142+156+170+184), biphenyls (m/z 168+182) and phenanthrenes (m/z 178+192+206). The list of identified compounds is shown in Table 4. The numbers above peaks indicate carbon numbers of *n*-alkanes, MN - methylnaphthalenes, DMN - dimethylnaphthalenes, TMN - trimethylnaphthalenes, TeMN - tetramethylnaphthalenes, MB - methylbiphenyls, DMB - dimethylbiphenyls, P -phenanthrene, MP - methylphenanthrenes, DMP - dimethylphenanthrenes.

Table captions

Table 1.

The most intensive compounds identified in the pyrograms and their relative abundances.

Table 2

Assignment of vibrational modes for the ATR-FTIR and FT Raman spectra of the studlovite samples (according to [9,10,20,22,23]).

ν - stretching, δ - deformation vibration, γ - out-of-plane, ρ - rocking, a - asymmetric, s - symmetric, ar - aromatic ring

Table 3

Results of the SEM/EDAX analysis of the samples studied.

*The results were averaged values obtained from four positions (see Supplemental material S2).

**The results were averaged values obtained from eight positions (Fig. 6A).

Table 4.

The most intensive compounds identified in the extracts and their relative abundances from the total ion chromatogram.

Table. 5

The main features and differences between studlovite I and studlovite II.

Characterization of Eocene fossil resin from Moravia, Czech Republic: Insights into macromolecular structure

Martina Havelcová^{a,*}, Vladimír Machovič^{a,b}, Alexandra Špaldoňová^a, Ladislav Lapčák^b,
Jiří Hendrych^b, Martin Adam^c

^a *Institute of Rock Structure and Mechanics AS CR, V Holešovičkách 41, 182 09 Prague 8, Czech Republic*

^b *Institute of Chemical Technology Prague, Technická 5, 166 28 Prague 6, Czech Republic*

^c *University of Pardubice, Faculty of Chemical Technology, Studentská 573, 532 10 Pardubice, Czech Republic*

1. Introduction

The Eocene epoch is known as a source of abundant accumulations of Baltic amber. This amber was transported from coastal areas of Northern Europe to the Mediterranean Sea in ancient times. The trade road, called the Amber Road, crossed the territory of Moravia, which has supported rich archaeological finds of amber [1,2]. However, next to Baltic amber, other amber occurrences were documented from deposits lying in Moravia, an area integral to the Czech Republic [3].

One of the Eocene amber deposits in Moravia is from the Carpathian Flysch Belt. This amber was entitled studlovite, according to its site of discovery at the village of Študlov, near Valašské Klobouky. Historically, findings of pieces of relatively high weight (> 40 grams) and up to 8 cm in size have been documented in the locality. Nowadays, occurrences are scarce. Colour and quality resembles Baltic amber, and the rare occurrence of suffused insects has also been documented [4].

Studlovite has been analysed in the past and it has been suggested that an angiosperm plant was the source of this amber [5]; a relationship with Baltic amber has also been proposed [6]. The most recent description of studlovite material [7,8] has revealed a chemical composition rather similar to that of the Cenomanian amber from Nové Strašecí.

Generally, amber is derived from exudates of conifers and certain angiosperms, and represents a valuable source of information about its botanical origins, ancient terrigenous ecosystems or distribution conditions. However, biochemical fingerprints of original resins have been modified during diagenesis, therefore the chemical analysis of amber is not straightforward. Biomarkers of fossil resins are terpenoids, and among them, specific terpenoids representing one plant family have the highest chemotaxonomic value. Such an identifying terpenoid has not been found for Študlov amber and doubts about the source of the original plant material still persist.

A more comprehensive geochemical analysis of the amber is therefore needed in order to evaluate the original plant source and the fossilization process. The aim of this study was to determine the molecular composition of Študlov amber using attenuated total reflection Fourier transformed infrared spectroscopy (ATR-FTIR), and Fourier transformed Raman spectroscopy, together with gas chromatography/mass spectroscopy and pyrolysis–gas chromatography/mass spectrometry (GC/MS and Py-GC/MS). Environmental scanning electron microscopy coupled with energy-dispersive X-ray analysis (SEM/EDAX) provided information on the elements present in the organic matter.

2. Materials and methods

2.1. Samples

The studlovite samples (studlovite I, studlovite II) were found in deep-sea sediments in a site formed by russet clay sandstone (Fig. 1). Amber pieces examined in this study were small in size ($0.5 \times 0.5 \times 0.5$ cm). The samples were brown in colour, partly transparent, one of them (studlovite II) having visible layers. They exhibited similar elemental compositions, having 69.7 wt% C, 8.1 wt% H, and below 0.1 wt% of N and S.

The locality of fossil resin at Študlov in eastern Moravia is a part of the Outer West Carpathians, which are made of Mesozoic and Tertiary flysch formations, the Carpathian Flysch Belt, and the locality lies in the deep-sea sediments of the Beloveža formation of the Račanská unit. The geological composition of the Račanská unit includes stratified sandstone, alternating with a conglomerate and inter-layered clay-slate, green-grey and red-brown claystone (upper Eocene, lower Oligocene).

2.2. Methods

The elemental organic composition of crushed and homogenized samples was determined using a CHNS/O micro-analyzer (Thermo Finnigan Flash FA 1112).

The sample (cca 0.2 mg) was dissolved in dichloromethane and analyses were performed using a Trace GC Ultra-DSQ II (ThermoElectron) instrument equipped with a TR-5MS column ($60\text{m} \times 0.25\text{mm} \times 0.25\mu\text{m}$). The oven temperature was programmed from 40 °C (1 min) to 120 °C (15 °C/min), to 200 °C (10 °C/min), then to 300 °C (10 min) (20 °C/min). The sample extracts were injected in splitless mode, the injector temperature was set at 220 °C and helium was the carrier gas. Mass spectra were obtained by scanning from m/z 20 to 500 in full scan mode. For data processing, the Xcalibur software (ThermoElectron) was used. Components were assigned from retention times and comparisons with mass spectra from the National Institute of Standards and Technology spectral library. Selected ion monitoring (SIM) was also used as a mode of data acquisition. The area of each individual peak was divided by the total area of the integrated TIC and expressed as the relative abundance of the total area in percent.

Py-GC/MS analyses were performed using a Pyroprobe 5150 pyrolysis unit (CDS Analytical) connected to the GC/MS instrument described above. Samples of fossil resins were heated at 400 °C for 20 s. This temperature was chosen based on experimental results (see Supplemental material S1). The Py-GC interface was kept at the maximum allowed temperature of 350 °C. A TR-5MS column was used and the temperature program of the column was set from 40 to 120 °C at a rate of 20 °C/min, continued at a rate of 8 °C/min to 210 °C, and finished at a rate of 20 °C/min to 300 °C, holding for 5 minutes.

Micro-ATR-FTIR analysis (ATR mapping) employed a Nicolet 6700 spectrometer (Thermo Nicolet Instruments Co.) combined with a Thermo Continuum IR microscope. The system was equipped with a X-Y-Z motorised stage with incremental steps of 1 μm . A polished section was placed on the microscope stage and the area of investigation ($280 \times 3400 \mu\text{m}$) was selected through a 15 x objective. Spectra were acquired over a wavenumber range of $4000\text{-}650 \text{ cm}^{-1}$, from 64 scans, at a spectral resolution of 4 cm^{-1} . An ATR germanium crystal directly connected to the objective was used, resulting in investigated areas of about $40 \times 40 \mu\text{m}$. A step size of $40 \mu\text{m}$ was used (588 points were measured). Data collection and post-run processing were carried out using Nicolet Omnic Atlas imaging software.

FT-Raman spectra were obtained using a Nicolet 6700 instrument with the NXR 9650 FT-Raman module attached and $\text{Nd}^{3+}/\text{YVO}_4$ near infrared excitation at 1064 nm. Spectra were acquired over a wavenumber range of $3500\text{-}50 \text{ cm}^{-1}$, and ~~Spectra were~~ recorded at 4 cm^{-1} resolution from 1024 accumulated scans. A nominal laser power of about 0.1 W was used with a spot size of $50 \mu\text{m}$.

A Quanta 450 scanning electron microscope (SEM) was used to study the samples. The semi-quantitative chemical compositions of the samples were analysed using an energy-dispersive X-ray microanalyser (EDAX, Apollo X) attached to the SEM, with a 12.5kV excitation electron beam. The analysis was carried out on selected spots of the cut surface prepared from the samples.

3. Results

3.1. Qualitative characteristic of bulk samples

The Py-GC/MS method utilized heat to release all volatiles and to degrade compounds from their solid state by thermal cracking or hydrogen abstraction reactions. The results of Py-GC/MS analysis (Fig. 2) were close for both samples: a set of cyclo-compounds and *n*-alkanes were the products of thermal reactions, and other substituted benzene, naphthalene, and phenanthrene compounds were products of bond breaking fragmentation reactions. The fragments produced are assumed to be representative of the original non-volatile compounds. Megastigmatrienone and ionone were identified only in pyrograms of studlovite II.

The infrared microspectra of the two study samples (Fig. 3) showed marked differences in band intensities of oxygen functional groups in the spectral range between 3700 and 3100 cm^{-1} , where a broad envelope of hydroxyl groups stretching vibrations of alcohols and phenols was found. Band positions at 3460 and 3225 cm^{-1} indicated the presence of hydroxyl groups with different hydrogen bonding strengths. A higher content of these OH groups was detected in studlovite I.

The representative Raman spectra of the two amber samples analyzed were qualitatively similar (Fig. 54), and differed mainly in the intensities C-H and C=C bonds. The spectral range of 1830-1500 cm^{-1} , as for the infrared spectra, was curve fitted using the Gaussian-Lorentzian function (Fig. 45 B, D, and Table 2). Bands of carbonyl functional groups (~ 1670 , ~ 1700 and 1725 cm^{-1}), double bonds (1650 cm^{-1}) and aromatic C = C bonds (~ 1610 and $\sim 1570 \text{ cm}^{-1}$) were detected in this region.

Bands of stretching vibrations of carbonyl groups and C = C bonds were determined in the spectral region 1800-1500 cm^{-1} . For a more detailed analysis, this region was curve fitted using a mixed Gaussian-Lorentzian function (Fig. 45 A,C). Both samples contained two distinct bands of ketones/H-bonded esters at 1724 cm^{-1} , and carboxylic acids at $\sim 1700 \text{ cm}^{-1}$. The relative proportions of these functional groups were determined based on intensities related to the intensity of the deformation vibrations of the aliphatic C-H bonds at 1446 cm^{-1} (i.e., I_{1724}/I_{1446} and I_{1700}/I_{1446}) [9]. Ketones/ H-bonded esters had almost the same representation in both samples, whereas the COOH group content was almost doubled in the studlovite I. These data were obtained by scanning of polished sections over entire sample profiles, and secondary surface oxidation of the samples can be excluded. The bands of anhydrides (1770 cm^{-1}), conjugated carbonyls (1664 cm^{-1}), double C = C bonds (1642 cm^{-1}) and C = C aromatic rings ($\sim 1600 \text{ cm}^{-1}$) were also identified (Table 2).

Stretching vibrations of aliphatic C-H bonds in CH_3 , CH_2 , and CH groups were found in the range 3000-2700 cm^{-1} . The corresponding area of deformation vibrations was located at ~ 1450 and $\sim 1380 \text{ cm}^{-1}$. A relatively large number of overlapping bands in the 1300-900 cm^{-1} region belonged predominantly to stretching vibrations of C-O bonds in acids, phenols, alcohols and esters. Next to these were bands of deformation vibrations of OH and CH bonds, and stretching vibrations of ring C-C bonds.

~~The representative Raman spectra of the two amber samples analyzed were qualitatively similar (Fig. 5), and differed mainly in the intensities C-H and C=C bonds. The spectral range of 1830-1500 cm^{-1} , as for the infrared spectra, was curve fitted using the Gaussian-Lorentzian function (Fig. 4 B, D, and Table 2). Bands of carbonyl functional groups (~ 1670 , ~ 1700 and 1725 cm^{-1}), double bonds (1650 cm^{-1}) and aromatic C = C bonds (~ 1610 and $\sim 1570 \text{ cm}^{-1}$) were detected in this region.~~

Despite the organic origin of amber, the material also contained inorganic elements, as was demonstrated by SEM/EDAX analysis (Table 3).

There were differences between the samples in higher levels of Fe, Al, and Si in studlovite I, and higher levels of Pb in studlovite II.

3.2. Layer-by-layer amber characterisation

Microphotographs of studlovite II enhanced layers present in the amber structure are shown (Fig. 6A). A suitable rectangular area was sketched, with dimensions of 280 x 3400 μm and with 504 points. The area contained eight layers of irregular thickness ranging from 120 to 560 μm that were 2D mapped by infrared ATR microspectroscopy.

The spectra obtained on the layer boundaries demonstrated the presence of significantly higher concentrations of oxygen containing functional groups than regions within layers. Moreover, the specific band for carboxylic acids indicated their higher presence on the boundaries. Semi-quantitative aspects of the FTIR analysis was presented as ratios of the integrated areas of carbonyl groups, including aldehydes, ketones, carboxylic acid, carboxylate esters and anhydrides ($1800\text{-}1540\text{ cm}^{-1}$), and aliphatic bonds, represented by $\delta\text{-CH}$ deformation modes ($1505\text{-}1405\text{ cm}^{-1}$). For the detailed distribution of oxygen containing functional groups, the carbonyl groups in ketones/H-bonded esters (1720 cm^{-1}) and in carboxylic acids (1695 cm^{-1}) were applied as well. The resulting representations of the area ratio $A_{\text{C=O}}/A_{\text{C-H}}$ (Fig. 6B) and intensity ratio I_{1720}/I_{1695} (Fig. 6C) followed and highlighted the layer boundaries, showing that oxygen containing groups, specifically carboxylic acids, were present in higher concentrations on the layer interface. The material in regions between layers of the fossil resins was richer in aliphatic chains and ketonic C=O bonds.

From the profile, the highest concentrations of carbonyl groups were observed on both outside layers of the pieces studied, and therefore eight average spectra from the eight individual layers and the $I_{\text{C=O}}/I_{\text{C-H}}$ ratios were used for a more detailed analysis. The layer profile showed that the ketone/H-bonded ester concentrations were relatively constant in all layers while the concentration of carboxyl groups changed, with the highest concentrations occurring in the outer layers, and the lowest in the middle 4 to 6 layers (Fig. 7).

Layers of a piece of studlovite II also showed differing inorganic chemical signatures (Fig. 8A). The distribution of Na, Mg, Al, Si, and Fe was comparable among the layers with an important decrease in the fifth layer. But the inorganic signals in layers were different for Cu and Pb, which seemed to be quite homogeneous through the sample (Fig. 8B).

3.3. Solvent extract analysis

Samples had low extractability in dichloromethane: 3.6wt%, and 5.1wt% respectively.

The studlovite II sample extract contained high concentrations of aromatic compounds (65%), comprising substituted naphthalenes, biphenyls and phenanthrenes (Fig. 9 B, Table 4). $\text{C}_1\text{-C}_4$ methylnaphthalenes were dominant (46%) together with methylbiphenyls (15%). The saturated hydrocarbons included mainly *n*-alkanes (25%) with their distribution in the range from *n*- C_{10} to *n*- C_{28} , and with lower *n*-alkanes dominating with a maximum at *n*- C_{11} . The acyclic isoprenoid pristane (Pr) was also identified. The composition of the studlovite I sample extract differed noticeably from studlovite II with a very weak contribution of all compounds (Fig. 9 A, Table 4).

Selected ion monitoring enabled the detection of minor concentrations of compounds with a terpenoid skeleton from the original resin source. The composition of both extracts included ionene,

methylionenes, cadalene, 8 β (H)-labdane, and simonellite. The extract of studlovite I also contained an unknown sesquiterpene with a molecular weight of 204, and the studlovite II extract contained 1,4-dimethyladamnatane (C₁₂ adamantane), 5,6,7,8-tetrahydrocadalene (calamene), and retene.

4. Discussion

Amber is a fossilized tree resin and its chemical structure can be quite complex and diverse, and being of a resinous nature, is more or less soluble in an organic solvent. As amber matures over years, additional polymerization and isomerization reactions take place, as well as crosslinking and cyclization. The FTIR and Raman spectral data from analysis of the macromolecular structure of bulk studlovite II revealed the presence of carboxyl, hydroxyl, and ketone or H-bonded ester functional groups as well as single and double bonds. Generally, some spectral bands characterize the degree of maturation or degradation of an amber sample based on determinations of oxygen functional groups and the relative abundance of aliphatic and aromatic structures [10]. An indicator of immaturity is the Raman band at about 1650 cm⁻¹, assigned to the C=C stretching vibration of double bonds in methylene groups, because the elimination and loss of these bonds are the result of cross-linking of the resin material or by oxidative and maturation processes. The other important Raman band, revealing aliphatic C-H bending, appears at about 1450 cm⁻¹. The intensity ratio of the 1650 and 1450 cm⁻¹ bands was suggested to indicate the degree of maturation. Jehlička et al. [9] found that values of this ratio ranged between 0.48 and 0.81 for fossil resin specimens, differing in localities, paleoecological situations and geological ages, including Bohemian and Moravian fossil resins and Baltic (Eocene) and Lebanon (Cretaceous) ambers. The studlovite samples studied showed I₁₆₅₀/I₁₄₅₀ ratio values that were noticeable lower, at 0.31, and 0.39 respectively, showing a higher degree of polymerisation and maturation of these samples.

Next to the loss of double bonds in methylene groups, the fossilization of natural resins is accompanied by an increase in aromatic structures. Considering I₁₆₁₀/I₁₄₅₀ ratios representing the presence of aromatic C=C bonds, this ratio was more than 10 % higher for studlovite I, showing the differential and higher degree of oxidation/maturation in comparison with studlovite II. The content of carboxylic groups in bulk samples was also much higher (44%) in studlovite I than in studlovite II, as was visible in curve fitted ATR-FTIR spectra (Fig. 3A and C), showing a broader band at 1700 cm⁻¹ that was caused mainly by intermolecular H bonds in OH and COOH groups.

Remarkably similar differences in composition and maturation were observable from GC/MS analyses of amber extracts, despite the fact that studlovite I was less soluble in dichloromethane and the extract was poorer in compounds, indicating a higher degree of polymerization. The prevailing compounds, identified in both extracts, were nonspecific for chemotaxonomy, but slight traces of terpenoid compounds were detected: the sesquiterpenoid cadalane belongs to a class that is a common constituent of conifers; 8 β (H)-labdane is a part of bicyclic diterpenoids produced mainly by conifers, although they can also occur in angiosperms [11]; ionene and methyl ionene may be derived from labdanes during degradation processes; the adamantane skeleton of 1,4-dimethyladamnatane is the basic unit of diamondoids (geosynthetic compounds), and seems to originate from β -ionone, *n*-alkanes and polycyclic hydrocarbons, as was proven by synthesis under laboratory conditions from these organic precursors [12,13]. Aromatic biomarkers simonellite and retene are derived from compounds with tricyclic/tetracyclic compounds with abietane or phyllocladane carbon skeletons that commonly occur in both angiosperms and gymnosperms. Low concentrations of terpenoid compounds and the presence of components that are highly degraded diagenetic products without chemotaxonomic value are not sufficient evidence to assess the botanical source of the studlovite samples.

The natural precursors of studlovite were suggested to be deciduous trees [5], however this assumption was made on the basis of a missing succinic acid peak in the FTIR spectra and the presence of oleanane in the extract. The absence of angiosperm triterpenoids in studlovite I and studlovite II extracts rather demonstrated conifers to be the source of the amber. Modern plant families reported in the literature as possible sources of amber for the Eocene age are Araucariaceae, Cupressaceae s.l., Pinaceae and Podocarpaceae [14]. Py-GC/MS was primarily used to differentiate and classify fossil resins [15]. Cyclo-compounds, *n*-alkanes, substituted benzene, naphthalene, phenanthrene compounds, as well as megastigmatrienone and ionone are fragments from terpenoid structures that formed the macromolecular amber matrix [16,17] and were fragmented through cracking reactions during pyrolysis. These compounds are nonspecific and it is hardly possible to use these data to conclude the origin of a resin. It can only be suggested that studlovite belongs to amber classification Class 2 due to the presence of methylnaphthalenes and traces of cadalene and 8 β (H)-labdane.

Warm and humid conditions could increase resin exudation, as is known from recent forests in a warm subtropical or tropical climate. Studlovite is of Eocene age when northern European land was characterized by stable subtropical-tropical climates and the warmest climate in the Cenozoic Era. Resin, produced inside plants, was exuded from the plant (in direct defense against herbivores and pathogens or by physical damage), and accumulated on the trunk or limbs. Then it either dropped to the soil or remained within the secretory tissue of the tree, preserved within the trunk that became fossilized in the protective soil environment [14]. The transformation of resin into amber continues from the moment of secretion until its burial. Layers of resin can build up and harden to form amber fossil and amber pieces that have layers of diverse thickness, representing individual resin flows. They often contain remnants of insects that were trapped in its sticky embrace. Nel and Prokop [18] and Tkoč et al. [4] described Scatopsidae and Dolichopodidae (Insecta: Diptera) in Študlov amber. Layers with an irregular thickness were microscopically identified in studlovite II (Fig. 3). The layers can be assumed to have accrued *in situ* and not during sedimentation processes without access to air because of variations found at interfaces especially the presence of oxygen-containing functional groups.

Two types of oxidative degradation that had occurred during resin fossilization can be recognised in studlovite II thanks to the detailed layer analysis of this amber. The first process was primary oxidation that was expressed as the enrichment of carboxylic groups found on boundaries between layers (Fig. 6C). It seems that the time between individual resin flows was sufficient for the hydrolysis of esters on the open resin surface, as was characterised by higher intensities of the specific band for carboxylic acids relative to carbonyl groups [19]. Moreover, the carbonyl stretching vibration at 1720 cm⁻¹ was at a lower frequency than typically seen in aliphatic esters and this may be due to the polymeric structure of the resinite. The complex macromolecular structure could, for example, allow hydrogen bonding between ester and adjacent alcohol groups, thus lowering the carbonyl stretching frequency [20]. The secondary oxidation process, revealed in averaged spectra from the individual layers as decreasing concentrations of carboxylic groups towards the centre layer of the fossil resin, can be attributed to diffusion of the oxidation medium (air, water) into the reaction system.

After resin secretion, a first contact was with rainwater and eventually with seawater droplets that sprinkled the resin stuck on the tree trunk or covered in the forest litter. Sodium is assumed to be a typical marine element but no enrichment was observed in the samples, indicating that the inorganic signature was not influenced by a saline environment during amber formation, although sedimentological evidences indicated that the investigated samples were deposited in a deep-sea environment. Most of the elements determined, such as macro and micro nutrients, elements sensitive to redox conditions or those related to siliciclastic sources (Na, Mg, K, Fe, Si, Al) can be interpreted in terms of natural plant parts and biological processes. Being located beneath the soil, they were absorbed by plants and the resin composition can then be influenced by soil composition. The

distribution of inorganic elements in layers of studlovite II (Fig. 8A) showed that the concentrations of Na, Mg, Fe, Si, and Al reflected resin secretion that was gradually produced and affected by different conditions within the tree and in the soil. The interesting finding was the high lead content in studlovite II, without a significant fluctuation in concentration within the layers. In sedimentary rocks, lead distribution is controlled by the presence of primary detrital minerals (feldspar, mica, and sulphides), clay minerals and organic matter. Lead has a strong affinity for organic ligands and could be adsorbed onto the reactive surface sites on resin surfaces. The sorption might be attributed to resin carbohydrates and phenolic compounds that have metal-binding functional groups such as carboxyl and hydroxyl groups [21].

5. Conclusion

Analysis of the results showed that both studlovite samples were derived from the same plant source, with higher polymerisation and maturation of the fossilized matter. The samples alone, however, displayed differences in structure and chemical composition (Table 5). These variations could be ascribed to dissimilar processes when the structure of studlovite II was built by continuous resin layering that affected the resulting chemical composition of the amber. However, the final fossilisation of both samples lead to material with many nonspecific paleotaxonomic characteristics. Trace elements in amber samples could only demonstrate the paleoenvironmental conditions that existed in plants during resin exudation following wounding.

Acknowledgements

The work was carried out thanks to the Operational Program Prague—Competitiveness, project Centre for Texture Analysis (CZ.2.16/3.1.00/21538), and to the long-term conceptual development of research organisation RVO: 67985891. The authors are grateful to John Brooker for reviewing and correcting the manuscript.

References

- [1] V. Mátl, To the provenience of amber in archaeological excavations in Moravia, *Minerál* 1/93, (1993) 21 (in Czech).
- [2] I. Mrázek, Gemstones in prehistoric times in Moravia and Silesia, *Moravian Museum in Brno* 203 (1996) (in Czech, English summary).
- [3] M. Přichystal, Bernsteinbearbeitung in der hallstattzeitlichen Siedlung der Lausitzer Urnenfelderkultur in Kralice na Hané (Bez. Prostějov), *Urnfield and Hallstatt Periods, Contributions to the IXth conference in Bučovice 3.- 6. 10. 2006*, pp. 209–230 (in Czech, German summary).
- [4] M. Tkoč, A. Nel, J. Prokop, Discovery of a new species of the Cretaceous genus *Microphorites* Hennig, 1971 (Diptera: Dolichopodidae s. lat.) in Paleogene amber from eastern Moravia (Czech Republic), *Insect Syst. Evol.* 47 (2016) 181–193.
- [5] V. Mátl, J. Franců, Z. Boháček, O. Krejčí, Occurrence of amber in Študlov locality (Bílé Karpaty Mts., Moravia), *Bulletin mineralogicko-petrologického oddělení Národního muzea v Praze*, VII (1999) 179–183 (in Czech).
- [6] M. Ručka, P. Sláma, Unknown gemstone - retinit from Valašské Klobouky, *Minerál* 2/97 (1997) 115–121 (in Czech).

- [7] M. Havelcová, I. Sýkorová, K. Mach, Z. Dvořák, Organic geochemistry of fossil resins from the Czech Republic, *Procedia Earth and Planetary Science* 10 (2014) 303–312.
- [8] M. Havelcová, V. Machovič, M. Linhartová, L. Lapčák, A. Přichystal, Vibrational spectroscopy with chromatographic methods in molecular analyses of Moravian amber samples (Czech Republic), *Microchem. J.* 128 (2016) 153–160.
- [9] J. Jehlička, S.E. Jorge Villar, G.H.M. Edwards, Fourier transform Raman spectra of Czech and Moravian fossil resins from freshwater sediments, *J. Raman Spectrosc.* 35 (2004) 761–767.
- [10] C.W. Beck, E. Wilbur, S. Meret, Infra-red spectra and the origin of amber, *Nature* 201 (1964) 256–257.
- [11] A. Otto, V. Wilde, Sesqui-, di- and triterpenoids as chemosystematic markers in extant conifers – a review, *Bot. Rev.* 67 (2001) 141–238.
- [12] L. Berwick, R. Alexander, K. Pierce, Formation and reactions of alkyl adamantanes in sediments: carbon surface reactions, *Org. Geochem.* 42 (2011) 752–761.
- [13] A. Ma, Advancement in application of diamondoids on organic geochemistry, *J. Nat. Gas Geosci.* 1 (2016) 1–9.
- [14] J.H. Langenheim, *Plant resins*, Timber Press, Inc., Potland, Oregon, 2003.
- [15] K.B. Anderson, R.E. Winans, Nature and fate of natural resins in the geosphere. I. Evaluation of pyrolysis-gas chromatography mass spectrometry for the analysis of natural resins and resinates. *Anal. Chem.* 63 (1991) 2901–2908.
- [16] G. Fráter, J.A. Bajgrowicz, P. Kraft, Fragrance chemistry, *Tetrahedron* 54 (1998) 7633–7703.
- [17] M.-F. Nonier, N.V. De Gaulejac, N. Vivas, C. Vitry, Characterization of carotenoids and their degradation products in oak wood. Incidence on the flavour of wood, *CR Chim.* 7 (2004) 689–698.
- [18] A. Nel, J. Prokop, New Paleogene Scatopsidae (Diptera: Nematocera) in amber from the Czech Republic and France. *Acta Societatis Zoologicae Bohemicae* 68 (2004) 91–98.
- [19] G. Pastorelli, Y. Shashoua, J. Richter, Hydrolysis of Baltic amber during thermal ageing – An spectroscopic approach. *Spectrochim. Acta A* 106 (2013) 124–128.
- [20] G. Socrates, *Infrared and Raman characteristic group frequencies: Tables and chart*, 3rd ed., Wiley & Sons, 2004.
- [21] A.E. Ofomaja, E.B. Naidoo, Biosorption of lead(II) onto pine cone powder: Studies on biosorption performance and process design to minimize biosorbent mass, *Carbohydr. Polym.* 82 (2010) 1031–1042.
- [22] [M. Guiliano, L. Asia, G. Onoratini, G. Mille, Applications of diamond crystal ATR FTIR spectroscopy to the characterization of ambers, *Spectrochimica Acta A* 67 \(2007\) 1407–1411.](#)
- [23] [R.H. Brody, H.G.M. Edwards, A.M. Pollard, A study of amber and copal samples using FT-Raman spectroscopy, *Spectrochimica Acta A* 57 \(2001\) 1325–1338.](#)

Figure captions

Fig. 1. A - Amber piece at the exposure of the clay sandstone; B - studlovite I; C - studlovite II: layers are obvious in this transparent amber.

Fig. 2. Total ion pyrograms of studlovite I and studlovite II. The list of all identified compounds is in Table 1. The numbers above peaks indicate carbon numbers of *n*-alkanes, DMB - dimethylbenzene, TMB - trimethylbenzenes, DEB - diethylbenzene, N - naphthalene, MN - methylnaphthalenes, B - biphenyl, DPMB - diisopropylmethylbenzene, DPX - diisopropylxylene, M - megastigmatrienone, I - ionone, TeHP - tetrahydrotrimethylnaphthalene, diAdiPM - diacetyldiphenylnaphthalene, TeMP - tetramethylphenanthrene.

Fig. 3. ATR-FTIR microspectra of studlovite I and studlovite II. The list of bands and their assignments is in Table 2.

~~**Fig. 4.** Curve fitted ATR spectra of studlovite I (A) and studlovite II (C), and curve fitted Raman spectra of studlovite I (B) and studlovite II (D). The list of bands and their assignments is in Table 2.~~

Fig. 54. FT-Raman spectra of studlovite I (A) and studlovite II (B). The list of bands and their assignments is in Table 2.

~~**Fig. 45.** Curve fitted ATR spectra of studlovite I (A) and studlovite II (C), and curve fitted Raman spectra of studlovite I (B) and studlovite II (D). The list of bands and their assignments is in Table 2.~~

Fig. 6. A - Microphoto of a studlovite II amber piece with the area studied and 504 measured points (280 x 3400 μm), B - ATR-FTIR profile $A_{\text{C=O}}/A_{\text{C-H}}$ (1800-1540 cm^{-1} /1505-1405 cm^{-1}), C - ATR-FTIR profile I_{1720}/I_{1695} . (The white lines on B and C arose during sample cutting and polishing.)

Fig. 7. Relative representation of esters (1720 cm^{-1}) and carboxylic acids (1695 cm^{-1}) obtained using $A_{\text{C=O}}/A_{\text{C-H}}$ (1800-1540 cm^{-1} /1505-1405 cm^{-1}) ratios from averaged curve-fitted spectra in individual layers. R = aliphatic substituent or polymolecular fragment

Fig. 8. Distribution of inorganic elements within the layers of studlovite II.

Fig. 9. Total ion chromatograms (TIC) of studlovite I (A) and studlovite II (B) extracts, and selected ion monitoring chromatograms for *n*-alkanes (m/z 85), naphthalenes (m/z 128+142+156+170+184), biphenyls (m/z 168+182) and phenanthrenes (m/z 178+192+206). The list of identified compounds is shown in Table 4. The numbers above peaks indicate carbon numbers of *n*-alkanes, MN - methylnaphthalenes, DMN - dimethylnaphthalenes, TMN - trimethylnaphthalenes, TeMN - tetramethylnaphthalenes, MB - methylbiphenyls, DMB - dimethylbiphenyls, P -phenanthrene, MP - methylphenanthrenes, DMP - dimethylphenanthrenes.

Table captions

Table 1.

The most intensive compounds identified in the pyrograms and their relative abundances.

Table 2

Assignment of vibrational modes for the ATR-FTIR and FT Raman spectra of the studlovite samples (according to [9,10,20,22,23]).

ν - stretching, δ - deformation vibration, γ - out-of-plane, ρ - rocking, a - asymmetric, s - symmetric, ar - aromatic ring

Table 3

Results of the SEM/EDAX analysis of the samples studied.

*The results were averaged values obtained from four positions (see Supplemental material S2).

**The results were averaged values obtained from eight positions (Fig. 6A).

Table 4.

The most intensive compounds identified in the extracts and their relative abundances from the total ion chromatogram.

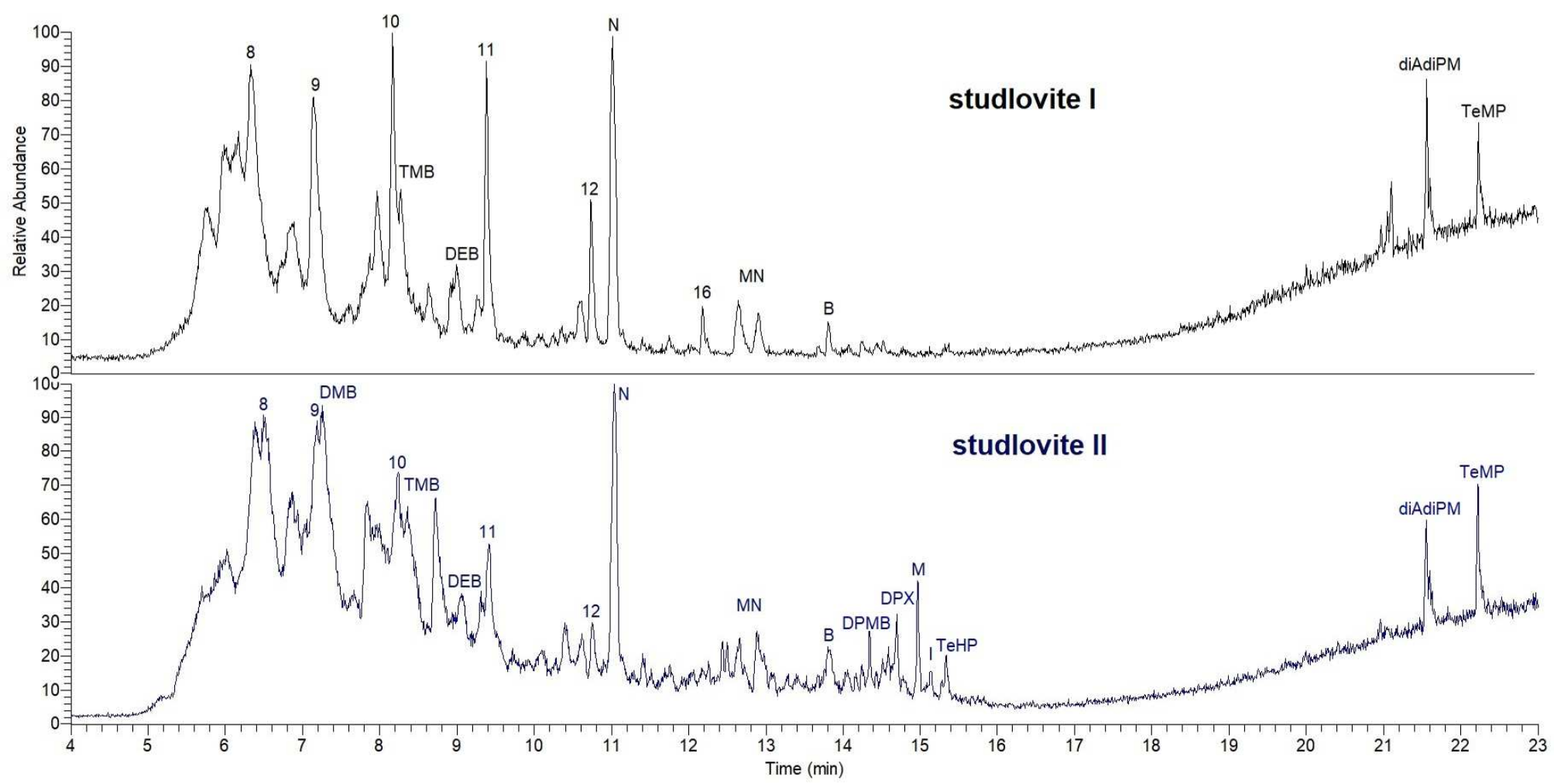
Table. 5

The main features and differences between studlovite I and studlovite II.

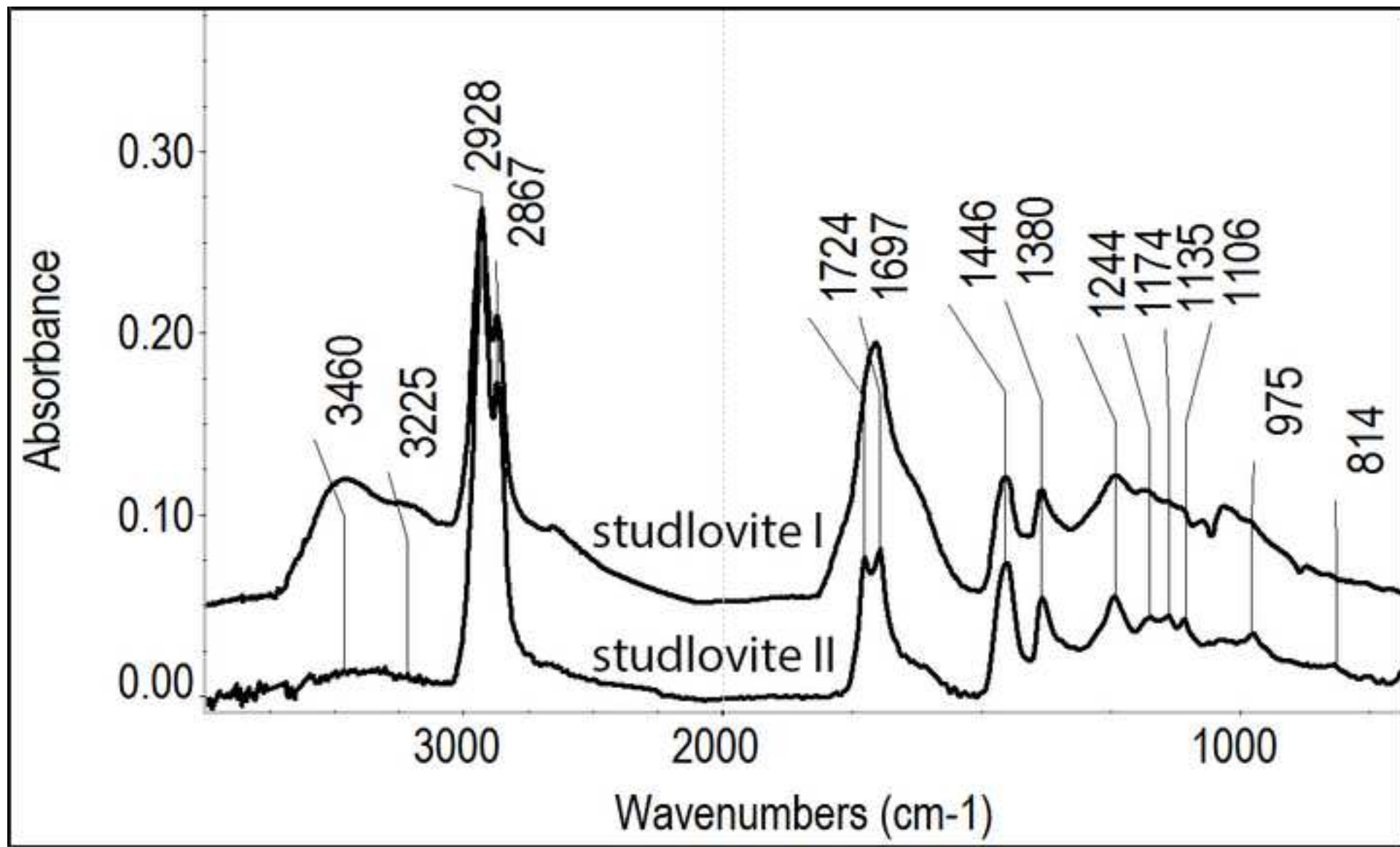
Figure(s) 1
[Click here to download high resolution image](#)



Figure(s) 2

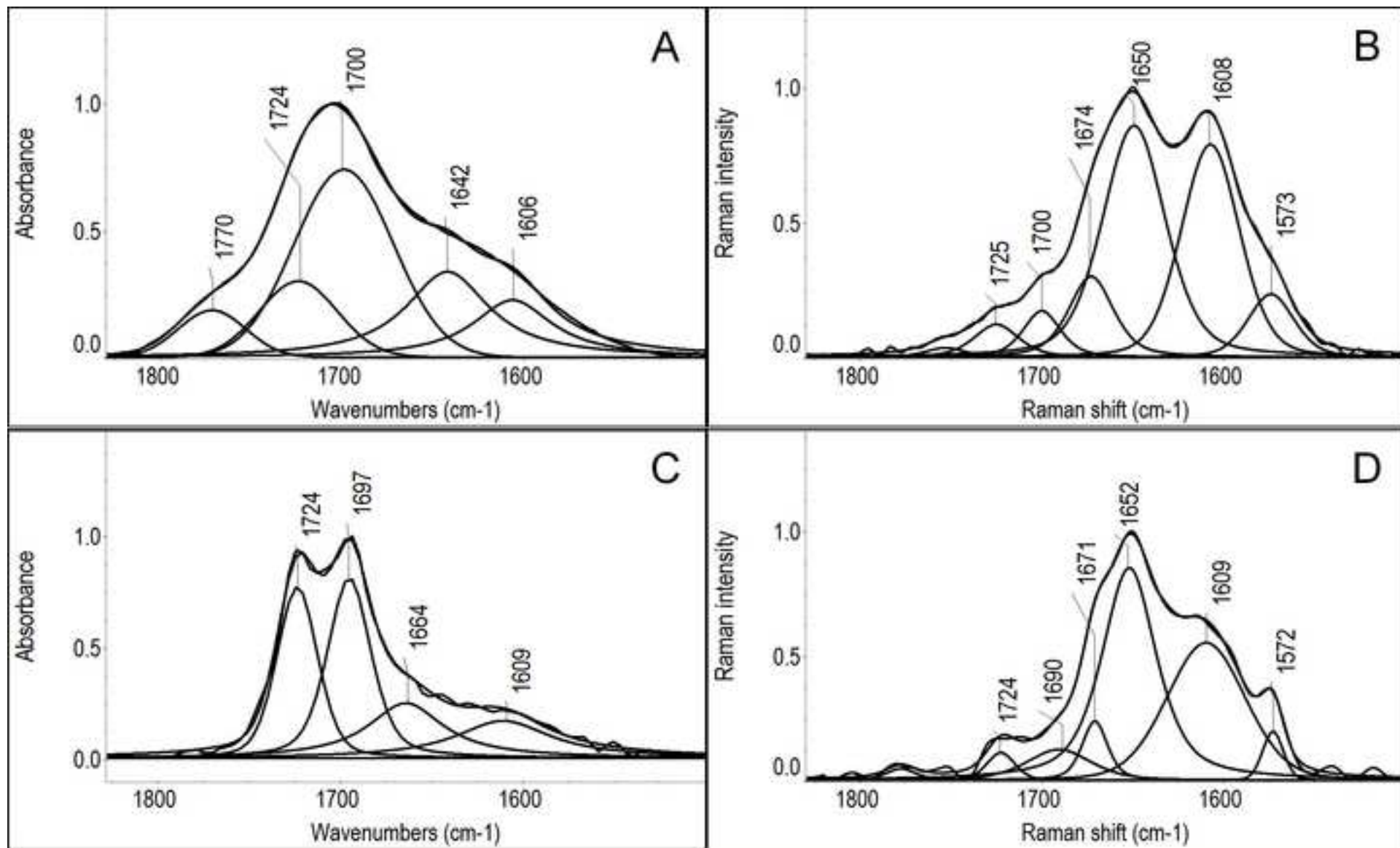


Figure(s) 3
[Click here to download high resolution image](#)



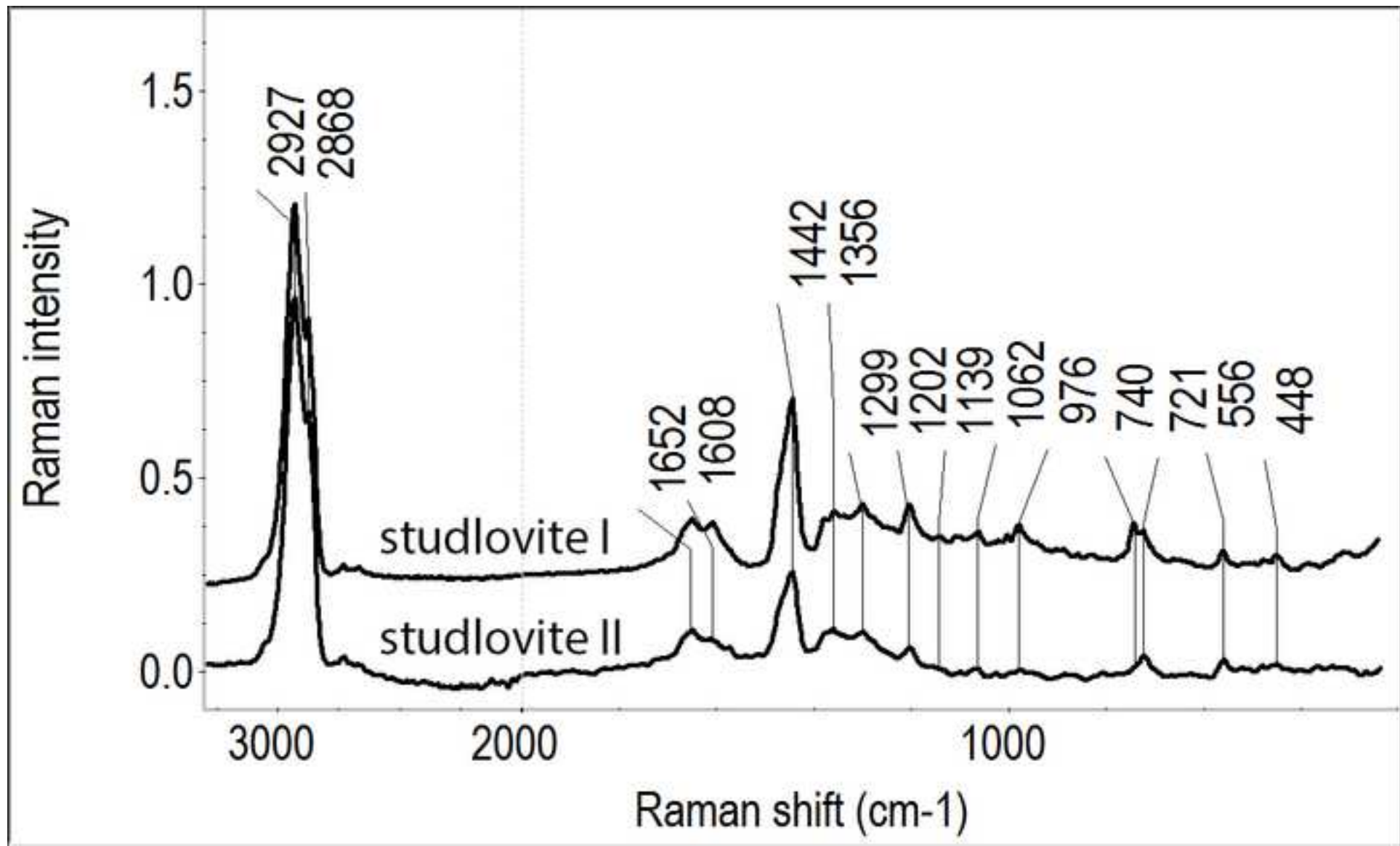
Figure(s) 4

[Click here to download high resolution image](#)



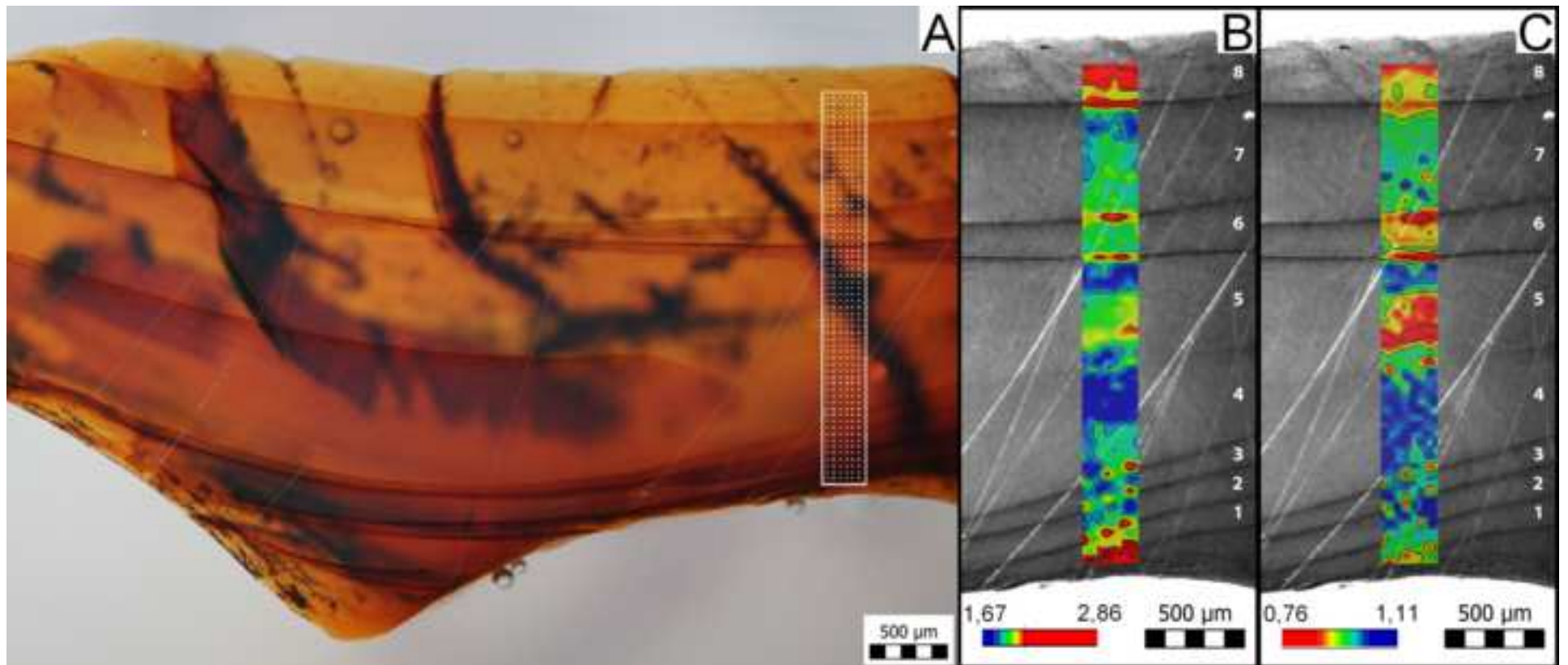
Figure(s) 5

[Click here to download high resolution image](#)

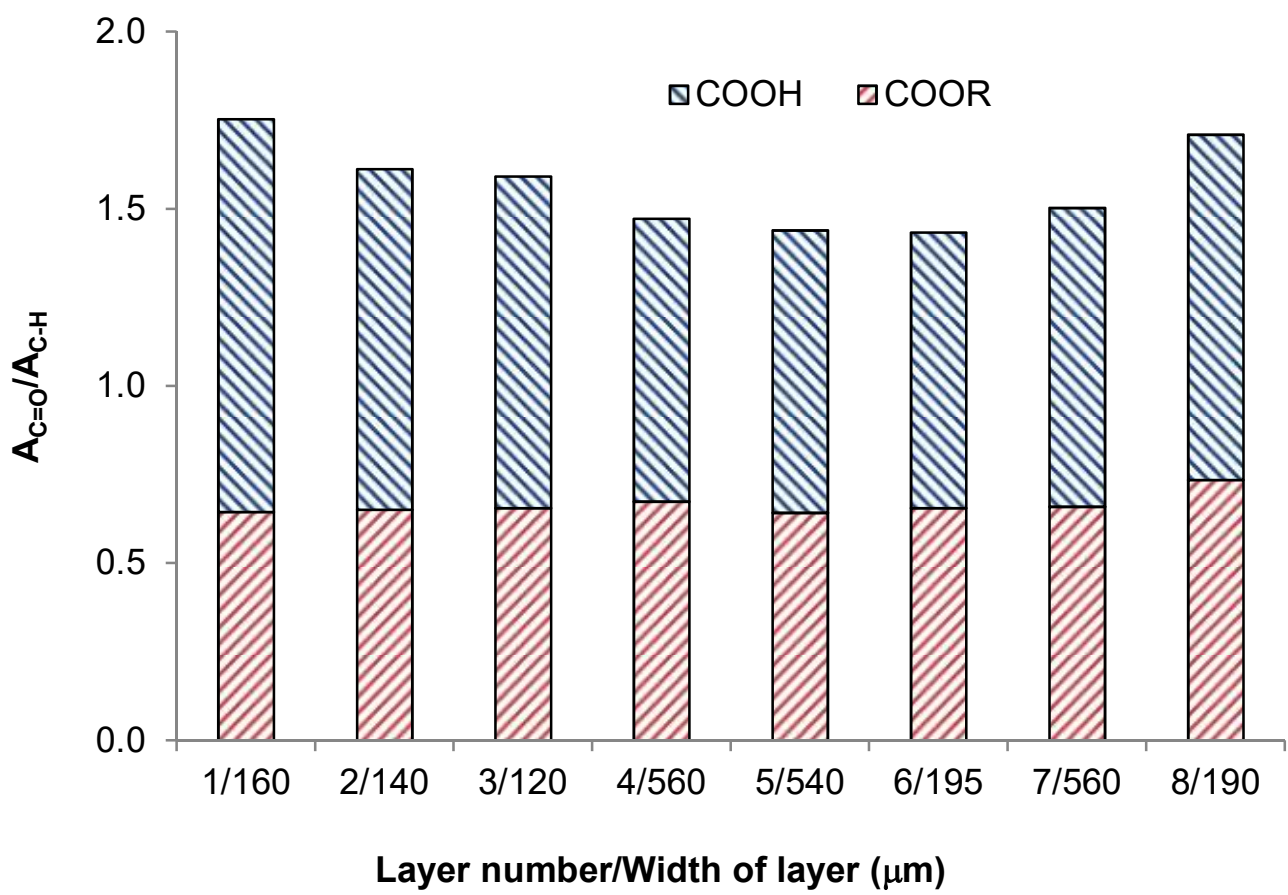


Figure(s) 6

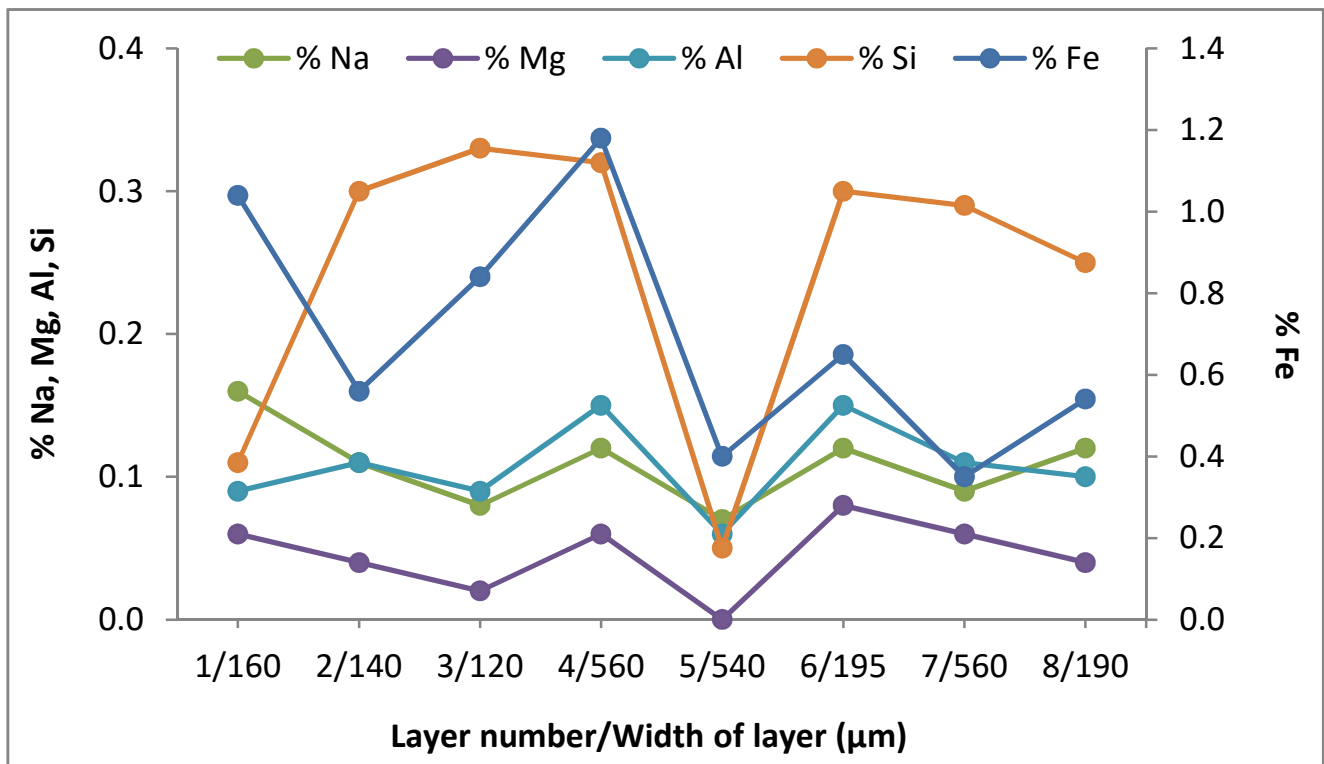
[Click here to download high resolution image](#)



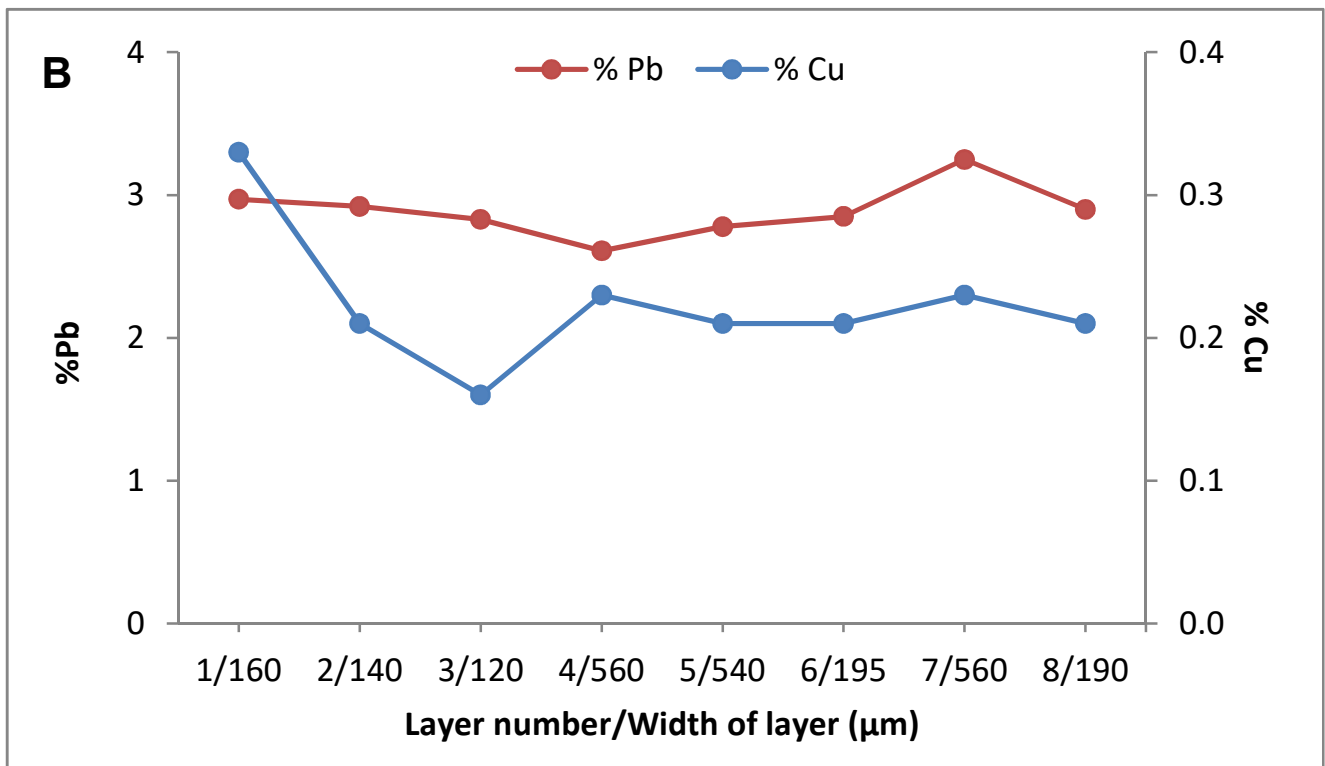
Figure(s) 7



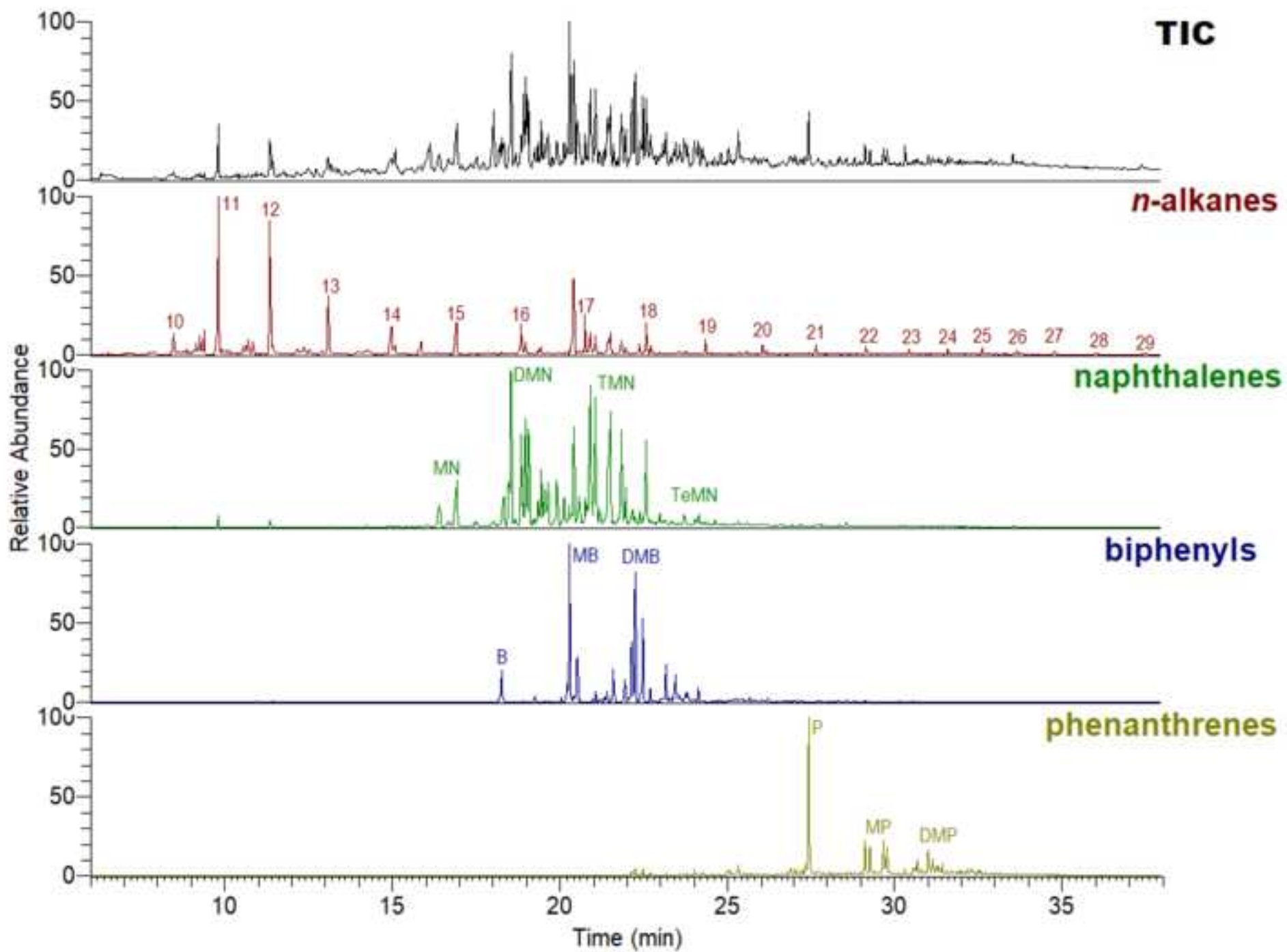
Figure(s) 8A



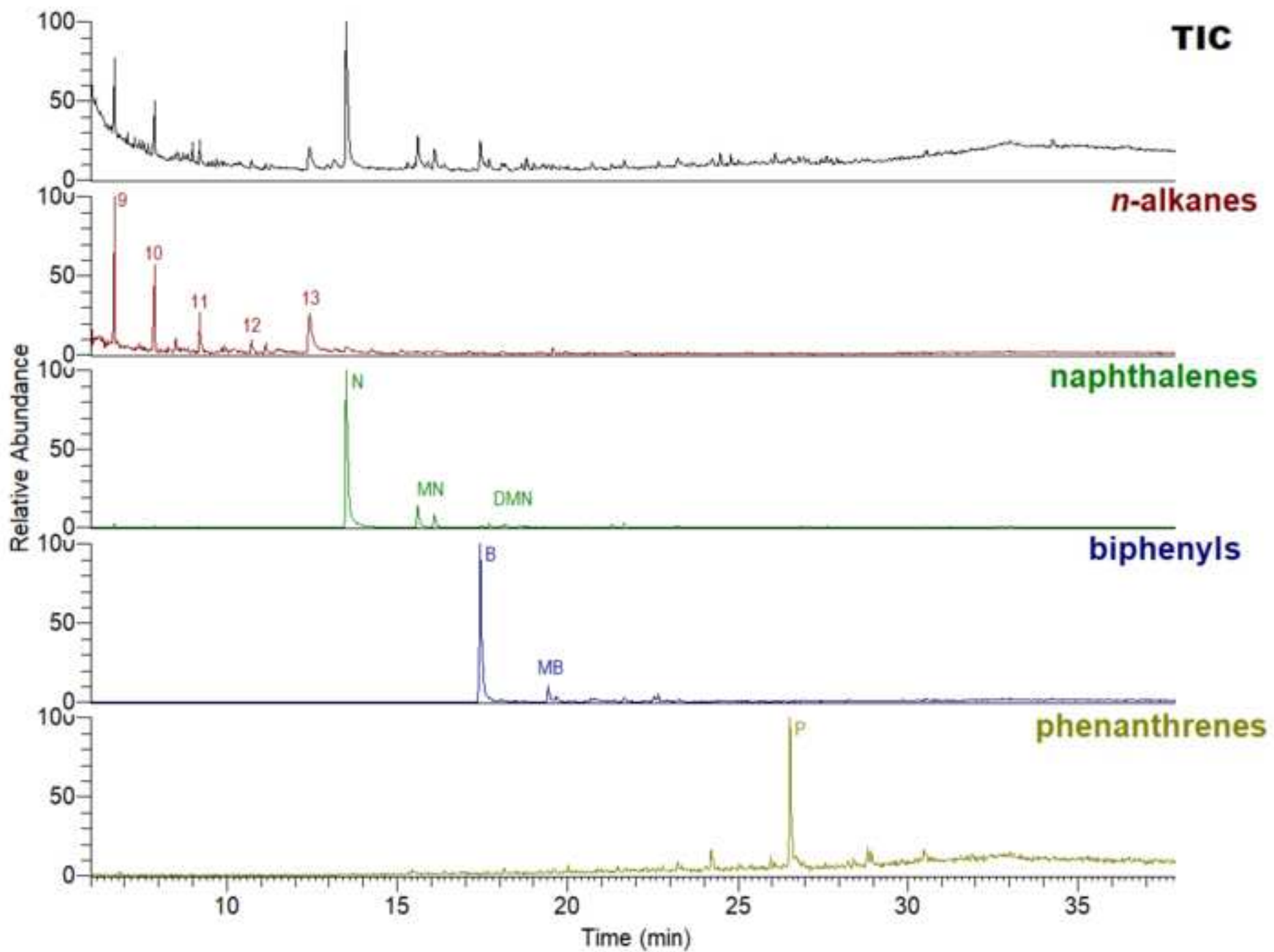
Figure(s) 8B



Figure(s) 9A
[Click here to download high resolution image](#)



Figure(s) 9B
[Click here to download high resolution image](#)



Table(s) 1

Retention time (min)	Molecular weight	Formula	Compound	Relative content (%)	
				studlovite I	studlovite II
5.7	100	C ₇ H ₁₆	<i>n</i> -C ₇	5.4	
6.0	98	C ₇ H ₁₄	methylcyclohexane	5.1	
6.4	96	C ₇ H ₁₂	dimethylcyclopentene		8.3
6.5	114	C ₈ H ₁₆	<i>n</i> -C ₈	10.8	8.4
6.9	110	C ₈ H ₁₄	dimethylcyclohexene	3.1	5.4
7.1	128	C ₉ H ₂₀	<i>n</i> -C ₉	14.0	5.7
7.3	106	C ₈ H ₁₀	dimethylbenzene		14.0
8.0	120	C ₉ H ₁₂	trimethylbenzene	4.2	3.9
8.2	142	C ₁₀ H ₂₂	<i>n</i> -C ₁₀	8.5	3.9
8.3	120	C ₉ H ₁₂	trimethylbenzene	2.8	2.3
8.6	120	C ₉ H ₁₂	trimethylbenzene	1.3	9.1
9.0	134	C ₁₀ H ₁₄	diethylbenzene	4.8	2.4
9.4	156	C ₁₁ H ₂₄	<i>n</i> -C ₁₁	9.5	4.3
10.7	170	C ₁₂ H ₂₆	<i>n</i> -C ₁₂	4.8	2.0
11.0	128	C ₁₀ H ₈	naphthalene	14.6	13.9
12.2	184	C ₁₆ H ₃₄	<i>n</i> -C ₁₆	1.2	
12.6	142	C ₁₁ H ₁₀	methylnaphthalene	3.4	1.5
12.9	142	C ₁₁ H ₁₀	methylnaphthalene	2.0	1.9
13.8	154	C ₁₂ H ₁₀	biphenyl	1.0	1.6
14.3	176	C ₁₃ H ₂₀	diisopropylmethylbenzene		1.3
14.7	190	C ₁₄ H ₂₂	diisopropylxylene		1.5
15.0	190	C ₁₃ H ₁₈ O	megastigmatrienone		2.8
15.2	192	C ₁₃ H ₂₀ O	ionone		0.6
15.3	174	C ₁₃ H ₁₈	tetrahydrotrimethylnaphthalene		1.0
21.6	252	C ₁₇ H ₁₆ O ₂	diacetyldiphenylmethane	2.2	2.0
22.2	234	C ₁₈ H ₁₈	tetramethylphenanthrene	1.4	2.3

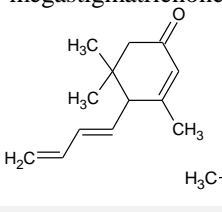
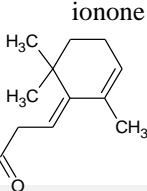
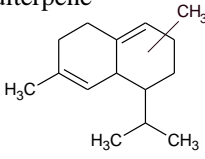
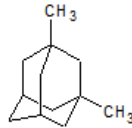
ATR-FTIR		FT Raman		Assignments
studlovite I	studlovite II	studlovite I	studlovite II	
3460, 3225	3450			$\nu(\text{O-H})$
2957	2957	2954	2954	$\nu^{\text{as}}(\text{CH}_3)$
2928	2928	2927	2927	$\nu^{\text{as}}(\text{CH}_2)$
		2893	2893	$\nu(\text{CH})$
2867	2867	2868	2868	$\nu^{\text{s}}(\text{CH}_3)$
2846	2846	2847	2847	$\nu^{\text{s}}(\text{CH}_2)$
1768				$\nu(\text{C=O})$ in anhydrides
1725	1724	1725	1724	$\nu(\text{C=O})$ in ketones
1702	1697	1707	1690	$\nu(\text{C=O})$ in COOH
	1664	1674	1671	$\nu(\text{C=O})$ conjug.
1649		1650	1652	$\nu(\text{C=C})$
1608	1609	1608, 1573	1609, 1572	$\nu(\text{C=C})_{\text{ar}}$
1446	1446	1465, 1442	1464, 1442	$\delta_{\text{s}}(\text{CH}_2)$, $\delta(\text{CH}_3)$
1380	1380	1384, 1356	1376, 1360	$\delta(\text{CH}_3)$
	1318, 1301	1299	1300	$\delta(\text{CH}_2)$, $\delta(\text{CH}_3)$
1274	1275			$\nu(\text{C-O})$, $\delta(\text{CH}_2)$, $\delta(\text{CCH})$
1244	1244			$\nu(\text{C-O})$, $\delta(\text{CCH})$
1174	1174	1202	1201	$\nu(\text{C-O})$, $\delta(\text{CCH})$, $\nu(\text{CC})$
1135	1135	1139		$\nu(\text{C-O})$, $\nu(\text{CC})$
1106	1106	1098	1098	$\nu(\text{C-O})$
1065	1065	1061	1062	$\nu(\text{C-O})$ sec. alcohols, $\nu(\text{CC})$
1037	1037, 999	1001	1024	$\nu(\text{C-O})$ prim. alcohols, $\nu(\text{CC})$
975	975	976	975	$\rho(\text{CH})$, $\gamma(\text{O-H})$ in COOH, $\nu(\text{CC})$
944, 929, 904	944, 929, 904	939		$\rho(\text{CH})$, $\gamma(\text{O-H})$ in COOH, $\nu(\text{CC})$
870	870	885	883	$\rho(\text{CH}_2)$, $\delta(\text{CH}_3)$, $\gamma(\text{C-H})_{\text{ar}}$
854	854	856		$\rho(\text{CH}_2)$, $\delta(\text{CH}_3)$, $\gamma(\text{C-H})_{\text{ar}}$
814	814	828	805	$\rho(\text{CH}_2)$, $\delta(\text{CH}_3)$, $\gamma(\text{C-H})_{\text{ar}}$
750	794, 750,	740		$\rho(\text{CH}_2)$, $\delta(\text{CH}_3)$, $\nu(\text{CC})$, $\gamma(\text{C-H})_{\text{ar}}$
722	722	721	719	$\rho(\text{CH}_2)$, $\nu(\text{CC})$
		556	555	$\delta(\text{CCO})$, $\nu(\text{S-S})$
			519	$\nu(\text{COC, S-S})$
		473, 448	446	$\delta(\text{CCO})$
		386	363, 332	$\delta(\text{CCO})$
		310	311	$\delta(\text{CCO})$

Table(s) 3

	% Fe	% Cu	% Na	% Mg	% Al	% Si	% P	% Pb	% K
studlovite I*	4.38		0.06	0.28	3.53	5.46			0.75
<i>RSD (%)</i>	4.6		11.3	4.7	1.1	0.5			1.3
studlovite II**	0.70	0.22	0.11	0.05	0.11	0.24	1.18	2.89	
<i>RSD (%)</i>	19.9	14.3	11.1	6.0	4.9	1.3	10.6	2.4	

Table(s) 4

Retention time (min)	Molecular weight	Formula	Compound name	Relative contents (%)	
				studlovite I	studlovite II
3.7	128	C ₉ H ₁₈	<i>n</i> -C ₉	6.9	
4.6	142	C ₁₀ H ₂₂	<i>n</i> -C ₁₀	5.3	2.8
5.7	156	C ₁₁ H ₂₄	<i>n</i> -C ₁₁	3.4	5.8
6.5	128	C ₁₀ H ₈	naphthalene	37.8	
6.6	164	C ₁₂ H ₂₀	1,4-dimethyladamanatane		1.1
6.7	170	C ₁₂ H ₂₆	<i>n</i> -C ₁₂	2.5	3.8
7.7	184	C ₁₃ H ₂₈	<i>n</i> -C ₁₃	6.9	1.6
7.9	142	C ₁₁ H ₁₀	2-methylnaphthalene	5.3	1.3
8.1	142	C ₁₁ H ₁₀	1-methylnaphthalene	6.4	4.3
8.3	158	C ₁₂ H ₁₄	hexa-1,3-dienylbenzene		0.9
8.4	154	C ₁₂ H ₁₀	biphenyl	1.8	
8.7	174	C ₁₃ H ₁₈	cyclohexyltoluene		1.0
8.7	196	C ₁₄ H ₂₈	C ₁₄ alkene		1.1
8.8	198	C ₁₄ H ₃₀	<i>n</i> -C ₁₄	3.3	1.7
9.0	156	C ₁₂ H ₁₂	dimethylnaphthalene	7.4	0.6
9.0	156	C ₁₂ H ₁₂	dimethylnaphthalene	1.6	1.0
9.1	156	C ₁₂ H ₁₂	dimethylnaphthalene		4.0
9.2	174	C ₁₃ H ₁₈	cyclohexyltoluene		3.6
9.3	156	C ₁₂ H ₁₂	dimethylnaphthalene	0.4	5.5
9.3	156	C ₁₂ H ₁₂	dimethylnaphthalene		3.1
9.5	156	C ₁₂ H ₁₂	dimethylnaphthalene	2.3	3.0
9.7	170	C ₁₃ H ₁₄	isopropylnaphthalene		1.1
9.7	156	C ₁₂ H ₁₂	2-ethylnaphthalene		0.9
9.8	204	C ₁₅ H ₂₄	sesquiterpene	1.8	
9.9	212	C ₁₅ H ₃₂	<i>n</i> -C ₁₅	1.3	1.5
10.0	168	C ₁₃ H ₁₂	3-methylbiphenyl	1.1	5.9
10.1	168	C ₁₃ H ₁₂	4-methylbiphenyl		0.9
10.2	170	C ₁₃ H ₁₄	trimethylnaphthalene		2.6
10.5	170	C ₁₃ H ₁₄	trimethylnaphthalene		2.9
10.5	170	C ₁₃ H ₁₄	trimethylnaphthalene		2.8
10.7	170	C ₁₃ H ₁₄	trimethylnaphthalene		1.5
10.7	170	C ₁₃ H ₁₄	trimethylnaphthalene		1.3
10.9	170	C ₁₃ H ₁₄	trimethylnaphthalene		3.2
10.9	224	C ₁₆ H ₃₂	C ₁₆ alkene		1.0
11.0	226	C ₁₆ H ₃₄	<i>n</i> -C ₁₆	1.7	0.4
11.1	182	C ₁₄ H ₁₄	dimethylbiphenyl		0.9
11.1	182	C ₁₄ H ₁₄	dimethylbiphenyl		3.8
11.3	182	C ₁₄ H ₁₄	dimethylbiphenyl		3.0
11.4	182	C ₁₄ H ₁₄	dimethylbiphenyl		0.8
11.4	184	C ₁₄ H ₁₆	methylpropylnaphthalene		0.9
11.5	184	C ₁₄ H ₁₆	tetramethylnaphthalene		0.4
11.5	182	C ₁₃ H ₁₀ O	4-methyldibenzofuran		1.2
11.7	184	C ₁₄ H ₁₆	tetramethylnaphthalene		1.1
11.8	184	C ₁₄ H ₁₆	tetramethylnaphthalene		1.4

	studlovite I	studlovite II
Colour, structure	brown, partly transparent	brown, layered
Elemental analysis	69.7 %C, 8.1%H, >0.1 %N, >0.1%S	
Py-GC/MS		
typical compounds	naphthalene	dimethylbenzenes
interesting compounds		megastigmatrienone  ionone 
Micro-ATR-FTIR		
C=O ketones/H-bonded esters (ratio I_{1724}/I_{1446})	+ 2% more than in studlovite II	
COOH acids (ratio I_{1700}/I_{1446})	+ 44% more than in studlovite II	
FT-Raman spectroscopy		
C=C double bonds (ratio I_{1650}/I_{1450})	0.31	+ 21% more than in studlovite I 0.39
C=C_{ar} aromatics (ratio I_{1610}/I_{1450})	+ 10 % more than in studlovite II	
Solubility		
dichloromethane	3.6%	5.1%
GC/MS		
more intensive compounds	naphthalene	3-methylbiphenyl
interesting compounds	sesquiterpene 	1,4-dimethyladamantane 
SEM/EDAX		
elements with highest content	Fe, Al, Si	Pb

Supplementary Material

[Click here to download Supplementary Material: Supplementary material.docx](#)